Agatova A.R., Nepop R.K., Carling P.A., Bohorquez P., Khazin L.B., Zhdanova, A.N. Moska P. Last ice-dammed lake in the Kuray basin, Russian Altai: new results from multidisciplinary research. Earth-Science Reviews, 103183, 2020. https://doi.org/10.1016/j.earscirev.2020.103183

LAST ICE-DAMMED LAKE IN THE KURAY BASIN, RUSSIAN ALTAI: NEW RESULTS FROM MULTIDISCIPLINARY RESEARCH

Agatova A.R.[1, 2], Nepop R.K. [1, 2], Carling P.A. [3], Bohorquez, P.[4], Khazin L.B. [5], Zhdanova A.N. [1], Moska P. [6]

[1]VS Sobolev Institute of Geology and Mineralogy, Siberian Branch of Russian Academy of Sciences, Novosibirsk, Russia

[2]Ural Federal University, Yekaterinburg, Russia

[3]Geography and Environment, University of Southampton, UK

[4] Centro de Estudios Avanzados en Ciencias de la Tierra (CEACTierra), Universidad de Jaén, Jaén, Spain

[5]Institute of Geology and Development of Fossil Fuels, Moscow, Russia

[6]Institute of Physics, Silesian University of Technology, Gliwice, Poland

Abstract

Results from geomorphological, sedimentological and geochronological analyses, together with micropaleontological and mineralogical characteristics of lacustrine deposits in five locations within the Kuray intermountain depression, southeast Altai, Mountains of south Siberia, support the thesis of repeated formations of ice-dammed lakes during MIS-2 and their draining by high energy floods. Our data suggest that the timing of one of the last cataclysmic draining events in the area can be estimated by an Optically-Stimulated Luminescence (OSL) age of 19.0 ± 1.1 ka for a sandy layer at the top of the diluvial (i.e. large flood) deposit, revealed in a sedimentary sequence of the 1570 m a.s.l. strandline – one of the lowest preserved strandlines in the western part of the basin. New OSL and radiocarbon ages, augmenting previously published dates, indicate that the last lake to occupy the Kuray depression occurred around 19–16 ka with a depth of at least 170 m in the

central part of the basin and to a depth of no less than 220 m near the glacier dam. Lacustrine deposits are represented by two horizons of sandy clays separated by interlayers of mixed-size sands. The mineralogical data, supported by analysis of sedimentological and micropaleontological records, indicate accumulation of a lower lacustrine horizon in a deeper reservoir. Finding of *Leucocythere* sp.1, *Leucocythere* sp.2, and *Leucocythere dorsotuberosa* ostracod species in lacustrine deposits characterizes these reservoirs as periglacial freshwater cold and deep lakes. The presence of well-crystallized mica and chlorite in lacustrine silts and clays from the lower lacustrine horizon indicates cold, dry conditions at the time of their formation, as well as a predominance of physical weathering of rocks within the denudation area. After an abrupt dropping of the lake level around 16 ka, determined from OSL dating, the lake never recovered its former depth. The available radiocarbon ages for organic material in subaerial deposits within the study area and the new OSL ages suggest that the last ice-dammed lake in the Kuray basin was drained between ~16.7 and 9.9 ka. The presence of this lake might explain the absence of late Paleolithic surface finds within the basin that remained generally unsuitable for human habitation until its final drying. The last outburst flood passed along the Chuya and Katun river valleys, which had been already carved by older cataclysmic floods, but did not significantly affect the topography downstream of the Kuray-Chuya intermountain depressions. We numerically simulated the draining of a palaeolake in the Kuray basin with the water level 1650 m a.s.l. (maximal depth about 220 m near the dam) with different scenarios of breaching the ice dam. In contrast to a relatively gradual breach of the ice dam due to thermal erosion, an instantaneous dam break due to structural failure can cause an outburst flood with a peak discharge of around 2×10^6 m^3 s^{-1}. The high speeds of the water flow, 1.9–5.6 m s^{-1}, with the maximum Froude numbers of 0.06–0.22, and peak Shields values of 0.03–0.25 indicate competence to mobilize gravel. Generally, the simulated flow remained subcritical, suggesting that bedforms developed under supercritical flows, such as antidunes, could not have developed, although the development of dunes cannot be precluded. Our data also contribute to the issue of

correlating the low lake strandlines in the Kuray basin with the landforms associated with cataclysmic outburst floods.

Keywords: ice-dammed lakes; cataclysmic outburst floods; ^{14}C dating; OSL dating; ostracods; numerical simulation; late Pleistocene; Holocene; Russian Altai.

1. Introduction

The Russian Altai, mountains of southern Siberia (**Fig. 1**), is one of the regions where extensive ice-dammed lakes were formed repeatedly in intermountain depressions during the Pleistocene glaciations. The subsequent warming led to degradation of ice dams and cataclysmic draining of these lakes. Significant landscape transformation took place as a result of such flood events. High-elevation lake strandlines, giant gravel dunes, lacustrine bars, overflow channels, specific erosional features (such as scabland topography), outwash deposits and fluvially-transported boulders provide evidence for and mark the pathway of the floods. Significant landscape changes occurred beyond the boundaries of these basins and extended over hundreds of km in the drainage valley network downstream of the ice-dam location.

The most famous intermountain depressions of Russian Altai, which hosted ice-dammed lakes, are the Kuray and Chuya basins (Butvilovsky, 1993; Baker et al., 1993; Carling, 1996a; Rudoy, 2002; Herget, 2005). At the time of maximal water filling of both basins, although separated by a mountain massif, the area was occupied by a giant single lake with a volume of about 607 km^3 and a surface area of 2630 km^2 (Herget, 2005). The presence of large ice-dammed lakes during the Pleistocene glaciations are also reconstructed for the Uimon intermontane basin (Butvilovsky and Prehtel, 2000; Bailagasov and Bailagasova, 2008; Rudoy and Rusanov, 2010; Zolnikov et al., 2016), Bertek basin (Groswald and Rudoy, 1996; Mikhailov and Redkin, 1997; Derevianko and Molodin, 2000), as well as assumed for some other smaller basins of the Russian Altai (Butvilovsky, 1993; Rudoy, 2005).

The estimated magnitude of the palaeofloods from the Kuray-Chuya system of basins range from an instantaneous peak discharge of 9–11 × 10^6 m^3 s^{-1} (Carling et al., 2010) for a partial breach of the ice-dam to about 20 × 10^6 m^3 s^{-1} for a complete dam removal (Bohorquez et al., 2016) and are considered to be among the largest known terrestrial fresh water discharges on Earth (Baker et al., 1993; Rudoy, 2005). The evidence of cataclysmic paleofloods in the Altai Mountains has encouraged extensive geomorphological, sedimentological, and palaeohydraulic studies to better

understand the processes and products of outburst floods (e.g. Butvilovsky, 1993; Baker et al., 1993; Carling, 1996a; Rudoy, 2002; Herget, 2005; Reuther et al., 2006; Zolnikov and Mistrukov, 2008; Carling et al., 2011; Bohorquez et al., 2016; Zolnikov et al., 2016).

Today the Pleistocene ice-dammed lakes within the Chuya-Kuray system of intermontane depressions and their cataclysmic drainage into the Arctic Ocean along the Ob river are among the most intensively studied of such phenomena in Central Asia. Nevertheless, the chronology of the Pleistocene Altai glaciations, as well as the chronology of associated ice-dammed lakes and their cataclysmic draining are highly debatable and in the next section we present a review of the major prevailing concepts. Among unsolved problems is the timing and duration of the last ice-dammed lakes, as well as how these lakes relate to the catastrophic outburst floods. Final drying of these last lakes in high-mountain depressions of the Russian Altai gave rise to the evolution of post-glacial landscapes, formation of the modern hydrological network, and settlement of the area by ancient people.

Our multidisciplinary study focuses on *i*) establishing the chronology of the last ice-dammed lake in the Kuray basin – the lower one in the Chuya-Kuray system of intermontane depressions; *ii*) estimating geomorphic parameters and ecological characteristics of this reservoir; *iii*) analyzing possible scenarios of its draining.

Another debatable issue, which is discussed in the paper, is the problem of correlating of specific landforms clearly expressed in the topography of the Kuray basin: *i*) low lacustrine strandlines – an indicator of relatively gradual draining of the last lake; and *ii*) giant gravel dunes with no lacustrine deposits within the basin's floor – prominent evidence of the cataclysmic character of the last outburst flood events.

2. Regional settings and history of investigations

The Altai Mountains are located within the northern part of the Central Asian Orogenic belt. They stretch northwest for more than 1500 km across the borders of Mongolia, China, Kazakhstan,

and Russia. The elevation decreases in the same direction from 4000 to 400 m a.s.l. (**Fig. 1**). The high-mountain southeastern part of the Russian Altai (SE Altai) includes the Chuya and Kuray intermontane depressions surrounded by ridges with altitudes in the range of 3500–4200 m a.s.l. The floor of the Chuya depression, the largest basin in the Altai Mountains, sits at 1750–2000 m a.s.l., while the floor of the Kuray depression lies at 1470–1600 m a.s.l.

Today the study area is characterized by a continental cryoarid permafrost environment. According to 77-year observations of the Kosh-Agach weather station the mean annual temperature is −5.2 °C (Weatherbase Kosh-Agach, Russia). The mean annual precipitation is less than 120 mm in the floor of the intermontane depressions, increasing significantly with height. The main moisture transfer is from the west (Atlantic Ocean) with the dominant influence of the Mongolian anticyclone in the east leading to increasing aridity southeastwards (Bohner, 2006). The mean annual precipitation near the snow line decreases in the same direction from 2000 mm in the western part of the Katun range to less than 500 mm in the Chikhachev range near the Mongolian border (Narozny and Osipov, 1999). The stony steppe on the floor of the Kuray depression grades into taiga vegetation on the slopes of the ranges. In the western mountains, flanking the Chuya depression, forests have an insular distribution, vanishing completely in the eastern part. The plateau-topped highlands are covered by arid mountain steppes. The higher topographic level is represented by alpine landscapes with mountain tundra and tundra-steppe vegetation changing with height into a glacial zone. In spite of the arid climate, the high altitudes of the ridges are favorable to modern glacier formation, although now they are rapidly shrinking (Pattyn et al., 2003; Galakhov et al., 2015; Ganiushkin et al., 2015).

The basic structure of the sedimentary fill of the Kuray depression was shown schematically by Butvilovsky (1993) (**Fig. 2**). He showed the principal correlation between Neogene deposits and Pleistocene lacustrine and diluvial deposits. Landforms associated with the Pleistocene ice-dammed lakes and their cataclysmic draining have been studied in detail (Carling, 1996a; Herget, 2005; Rudoy, 2005; Carling, 2013**)**.

The acceptance of the concept of glacial lakes outburst floods (GLOF) in Russia became possible after the identification and the investigation of GLOF landforms and sedimentary records in the Russian Altai (Butvilovsky, 1985, 1986; Rudoy, 1988; Rudoy and Baker, 1993). The cataclysmic character of the repeated outburst floods from ice-dammed reservoirs has been accepted by most researchers (Butvilovsky, 1993; Rudoy and Baker, 1993; Carling, et al., 2002; Rudoy, 2002; Herget 2005; Zolnikov and Mistrukov, 2008; Zolnikov et al., 2016). However, there remains an alternative concept of gradual, non-catastrophic drying of the Kuray and Chuya basins (Okishev, 1982; Novikov and Parnachev, 2000; Okishev and Borodavko, 2001; Pozdnyakov and Khon, 2001). These conflicting viewpoints require resolution.

The chronology of cataclysmic outburst floods as well as the chronology of the associated ice-dammed lakes are related closely with the timing of the Pleistocene glaciations. A geomorphological approach, assessing the state of preservation of ancient moraines, attempts to correlate glacial events and forms the basis for most paleogeographical reconstructions (Devyatkin, 1965; Butvilovsky, 1993). Morphologically distinct moraines of the maximal Middle- and two Late Pleistocene glaciations are evident in the SE Altai; the last glaciation being the smallest one (Devyatkin, 1965; Okishev, 1982; Agatova, 2005). In contrast, Butvilovsky (1993) supposed the last (MIS-2) glaciation in the SE Altai to be the largest, mainly on the basis of his observations in less-dissected areas of the NE Altai, where the glaciers during different Pleistocene glaciation epochs occupied practically the same area. Today only the surface effects of the last glaciation are most evidently expressed in the topography (Butvilovsky et al., 1991, 1996; Rudoy, 2002). Numerous radiocarbon dates provide the basis for the chronology of this glaciation (Butvilovsky, 1993). The presence of an earlier Pleistocene glaciation in the SE Altai was suggested by Svitoch et al. (1978) and Okishev (1982) on the basis of several thermoluminescence (TL) dates from the Chagan key section (see Agatova and Nepop, 2017a for review), and by Zykin et al. (2016) on the basis of finding boulders with glacial striation within the alluvial deposits of the Bashkaus Formation beneath moraines within the southern slopes of the Kuray range. Analyzing OSL dates of glaciolacustrine deposits in

the Uimon Basin, located in the headwater of the Katun River (**Fig. 1**), Zolnikov et al. (2016) proposed a MIS-5 (90–100 ka) age for the maximum of the latest glaciation, which may have caused the formation of the Uimon ice-dammed lake. OSL ages for silt on top of terminal moraines and in-between till deposits within the southeastern and the northwestern periphery of Chuya depression allowed Lehmkuhl et al. (2007) to date the last major ice advance as between 28 and 24 ka. Based on terrestrial cosmogenic nuclide dating of moraine boulders in the Chagan-Uzun valley Gribenski et al. (2016) suggested the Last Glacial Maximum in the SE Altai occurred at around 17–19 ka (see also Herget at al. 2017 for comments).

It could be stated that today there are generally three main concepts of the Pleistocene Altai glaciations: *i*) the Last Glaciation (Sartan according to Western Siberian glaciation scheme or MIS-2) was the largest among all Pleistocene glaciations and left the most prominent imprints in topography and sediments (Butvilovsky 1993; Rudoy, 2005); *ii*) the most extensive Middle Pleistocene glaciation was followed by two Late Pleistocene glaciations with the most recent being the smallest (Devyatkin 1965); *iii*) active interaction of glacier ice, icings and ground ice controlled by dry continental climate conditions, collectively indicating a unique Pleistocene glaciation in the region, where the first Late Pleistocene glaciation associated with cold substage MIS-5d was the largest one (Sheinkman, 2011).

Differences in perceptions of the number, chronology, and maximal extension of the Pleistocene Altai glaciations are closely related with the problems of the chronology and drainage mechanisms of cataclysmic outburst floods, as well as with the issues of sedimentation patterns downstream of the ice-dammed reservoirs along the Chuya and Katun river valleys. Regarding the last issue there are generally three main concepts for the formation of the high (traditionally called “Inya”, up to 300 m above the modern Katun River) and low (or “Saldzhar”, 50–100 m) complexes of terraces in Katun River valley, composed by megaflood sediments: *i*) implying the scheme of the Pleistocene Altai glaciations initially suggested by Butvilovsky (1993), both complexes of terraces - the lower, or the bed load terraces (deposited by bed-load transportation), and the upper, or giant

bars (deposited from suspension gravel of the outburst flood), were accumulated during MIS-2 events (detailed description and argumentation is presented in Herget (2005)); *ii*) based on the glaciation scheme developed by Devyatkin (1965), accumulation of the Inya and the Saldzhar sediment bodies occurred as a result of a series of megafloods over a relatively long time period – older (MIS-6 or MIS-8) and more powerful outburst floods produced the Inya terrace complex and later, weaker floods cut into it and embedded the much younger (MIS-4) sediments of the Saldzhar terrace complex (Zolnikov and Mistrukov, 2008; Krivonogov et al., 2017): no high-energy outburst floods were triggered in MIS-2; *iii*) applying the glaciation scheme of Devyatkin (1965) and numerous OSL dates, Panin and colleagues (Panin and Baryshnikov, 2015; Panin et al., 2015a) suggested that the most powerful floods occurred during MIS-4 and that more recent (MIS-2) outburst floods can also be characterized as high-energy events, that were not, however, so energetic.

Following different Pleistocene glaciation schemes there are also several chronological reconstructions of the ice-dammed lakes in the Chuya-Kuray basins. Using ^{14}C data, as well as two TL ages reported by Sheinkman (1990), Okishev and Borodavko (2001) suggested three lacustrine stages within the time interval of about 46–12 ka BP. More recently, OSL dates were used for reconstructing the formation of ice-dammed lakes in the Kuray basin at about 18.2 ka BP (Panin et al., 2015b) with a small residual lake in the western part of the basin at ~14.4 ka BP (Zolnikov et al., 2016). More detailed review on the topic is presented in Herget et al (2020).

Regarding the most important (in context of this paper) issue of the last ice-dammed lakes formation, and analyzing all available meagre dating data, a number of different views is promulgated: *i*) in the upper reaches of the Chuya River the last shallow reservoirs existed as two separate lakes in the Kuray (up to 20–30 m deep) and Chuya (50–70 m deep) basins at the end of MIS-2 (about 12–14 ka BP). Draining of these reservoirs is not believed to be associated with cataclysmic outburst floods (Okishev and Borodavko, 2001); *ii*) a conjoined water-body, the largest lake (water level up to 2100 m a.s.l. and with a depth of ~650 m near the dam), occupied the Chuya-

Kuray basins during MIS-2 (Herget, 2005), and its cataclysmic draining occurred around 18 ka (Gribenski et al. (2016): age calculated using ^{10}Be data reported by Reuther et al. (2006)). This last flood caused the accumulation of giant gravel dunes in the basins and spectacular giant bar deposits occurred in the valleys of the Chuya and Katun Rivers. In this scenario, an apparent draining event from the Uimon Basin was modelled as the backwater flooding into the basin from a flood from the Chuya-Kuray basins (Carling et al., 2010; Bohorquez et al., 2016; Bohorquez et al., 2019b); *iii*) alternatively, independent damming and cataclysmic draining of the Uimon depression in the upper reaches of Katun River took place during a cold substage of MIS-5 (90–100 ka) as a separate event unrelated to the Chuya-Kuray draining events (Zolnikov and Mistrukov, 2008; Zolnikov, 2011; Krivonogov et al., 2017). The Chuya basin was dry in MIS-4, there were no ice-dammed lakes in Chuya, Kuray, and Uimon depressions during MIS-2. Significantly smaller floods occurred during MIS-2 only due to draining of moraine-dammed or landslide-dammed lakes (Zolnikov et al., 2016); *iv*) last ice-dammed lakes occupied Kuray basin in MIS-2 but were associated neither with the largest Pleistocene glaciations, nor the most powerful draining events. Outburst floods from these MIS-2 lakes were able to produce the last generations of gravel dunes and affected the downstream topography along the Chuya and Katun river valleys, but not as much as the more powerful ancient floods (Panin et al., 2015a, b; Agatova et al., 2019a).

3. Methods

Detailed geomorphological investigations and process analyses were based on the interpretations of aerial photographs, Landsat-TM images, topographic maps (1:25000), and field investigations including mapping of landforms and deposits of different origin. Selected outcrops in the Kuray basin were studied to examine the sediments and landforms associations. Suitable materials from key locations were sampled for OSL and radiocarbon dating, as well as for mineralogical and paleontological analyses. In addition, reported sedimentation patterns and numerical ages for deposits of various genesis within the study area were analyzed for making

paleogeographical and paleoenvironmental reconstructions of the last ice-dammed lake in the Kuray basin.

Lithofacies analysis was applied to understand the sedimentary environments and the origin of the exposed deposits. We describe the exposed sediments and classified them into clearly distinguished facies based on substantive composition, structural and textural characteristics, such as color, grain size, shape and particle orientations, degree of particle rounding and sorting, dip angle and thickness of bedding, deformation patterns. Further recognition of facies associations, examination of their spatial relationships and deduction of depositional processes for each facies were done by applying the results and experience of previous regional-scale investigations of Carling (1996a, 1999, 2013).

Analysis of the biological composition of the sediments, with the main focus on micropaleontological analysis, was used for reconstructing the paleoecology of the lakes and characterizing the paleoenvironmental conditions of the sedimentation. The method of aggregate group analysis of biological composition was developed originally for application to gyttja (Korde, 1960) and later was supplemented and used for other freshwater environments (Uspenskaya, 1986). Untreated samples were suspended in water and were observed under a microscope (×280–400 magnification); all encountered remnants of flora and fauna (fragments of vascular plants, cysts and skeletons of algae, sponge spicules etc.) were identified up to the lowest possible taxonomic level.

Among the hydrobionts preserved in the bottom sediments of paleolakes, ostracods were chosen for micropaleontological analysis. These small crustaceans with bivalve carbonate shells are one of the most widespread group of skeletal hydrobionts, and are found in almost all types of Pleistocene-Holocene freshwater habitats. Ostracods have a unique combination of population, morphophysiological, and ecological characteristics, such as a short life cycle, a high reproductive rate, excellent skeletal preservation for both adult and larval forms in fossil taphocenoses, resistivity to short-time environment changes, with ecological specializations for survival during prolonged time intervals, and selectivity to physical and chemical environmental conditions, including climatic

and salinity factors. Analysis of fossil ostracods allows reconstruction of the salinity, temperature and depth of a lake. In each studied profile every 5 cm of sediments were sampled. Ostracod shells were isolated from 100 g sediment samples in order to provide commensurate counts. The sediment samples were wet sieved through a 0.067 mm mesh screen and then air dried. Valves were identified under a Zeiss Stemi 2000 binocular. The secondary electron images of valves were acquired using a Tescan MIRA 3 LMU scanning electron microscope equipped with an INCA Energy 450 Xmax 80 (Oxford Instruments, Oxford, UK) microanalysis system. Analyses were carried out using an accelerating voltage of 20 keV, a beam current of 1 nA, and a beam size of 10 nm.

The mineral composition of lacustrine deposits was studied by X-ray diffraction (XRD) and infrared (IR) spectroscopy. This approach was successfully applied to the study of lake sediments located in various climatic zones and tectonic settings (Fagel et al., 2007; Li et al., 2008; Solotchina et al., 2009; Joussain et al., 2016; El Ouahabi et al., 2017). Modern methods of mathematical treatment of XRD patterns are essential for identification, crystallochemical typification and studies of the real structure and abundances of highly dispersed clay minerals in multi-component systems (Walker, 1993; Moore and Reynolds, 1997; Solotchina et al., 2002). Samples were gently ground with ethanol in an agate mortar, attached to a glass substrate and dried before the analysis. XRD curves were obtained on an automated DRON-4 diffractometer (CuKα radiation, graphite monochromator). Diffraction spectra of air-dried samples saturated with ethylene glycol were used to diagnose clay minerals. IR spectra in the wavenumber range of 400–4000 cm^{-1} were obtained on a Specord 75 IR device.

Two OSL samples were collected by driving steel tubes into the sandy sediment. In the laboratory, samples were prepared both for gamma spectrometry and luminescence measurements. High-resolution gamma spectrometry using a HPGe detector was used to determine the content of U, Th and K in the samples. Prior to these measurements, the samples were stored for three weeks to ensure equilibrium between gaseous ^{222}Rn and ^{226}Ra in the ^{238}U decay chain. Each measurement lasted for at least 24 hours. The activities of the isotopes present in the sediment were determined

using IAEA standards RGU, RGTh, RGK after subtracting background values from the detector. Dose rates were calculated using the conversion factors of Guerin et al. (2011). The method of Prescott and Stephan (1982) was used for the cosmic ray beta dose rate calculation. The average water content was assumed to be 18 ± 5%. For OSL measurements, sand-sized grains of quartz (90–200 μm) were extracted and standard chemical procedures applied (Aitken, 1998) in the following order: first the sediment samples were treated with 20% hydrochloric acid (HCl) and 20% hydrogen peroxide (H_2O_2) to remove carbonates and organic material. Next the quartz grains were separated using density separation with the application of sodium polytungstate solutions leaving grains of densities between 2.62 g cm^{-3} and 2.75 g cm^{-3}. The grains were sieved, before etching with concentrated hydrofluoric acid for 20 minutes. An automated Risø TL/OSL DA-20 reader was used for the OSL measurements of multi-grain aliquots, each weighing ~1 mg. The stimulation light source was a blue (470 ± 30 nm) light emitting diode array delivering 50 mW cm^{-2} at the sample (Bøtter-Jensen et al., 2000). The detection was through a 7.5 mm thick Hoya U-340 filter. Equivalent doses were determined using the single-aliquot regenerative-dose protocol (Murray and Wintle, 2000). To calculate the luminescence ages, the central age model of Galbraith et al. (1999) was applied.

To estimate the chronological limits of studied hydrological events and to understand the influx of organic material into sediments, four samples were collected for radiocarbon dating. ^{14}C ages were obtained by liquid scintillation counting (LSC) methods at the Institute of Geology and Mineralogy SB RAS, Novosibirsk (marked by the SOAN index) and at the Laboratory of radiocarbon dating and Electronic Microscopy of the Institute of Geography RAS, Moscow (marked by the IGAN index). The production of lithium carbide and benzene synthesis was completed using the standard technique (Arslanov, 1987; Skripkin and Kovaliukh, 1997). The activity of ^{14}C was determined using the Quasntulus-1220 liquid scintillation counters. All ^{14}C ages were calculated by applying $\delta^{13}C$ value of -25 ‰. The conventional ^{14}C ages were calibrated (2σ standard deviation) to calendar ages using the CALIB Rev 7.1 program (http://calib.qub.ac.uk/calib/) and the IntCal13

calibration data set (Reimer et al., 2013). The conventional radiocarbon ages were calibrated (2σ standard deviation) applying the CALIB Rev 7.1 program (http://calib.qub.ac.uk/calib/), with the IntCal13 calibration data set (Reimer et al., 2013). The paper presents both the conventional (years BP) and the calibrated (cal BP) ^{14}C ages.

The lake drainage model developed by Bohorquez et al. (2019b) was used to numerically simulate the draining of a palaeolake with the water level at 1650 m a.s.l. The purpose of this exercise was to estimate flow parameters above the 1570 m a.s.l. strandline, where the sedimentary sections have been investigated, and to evaluate if the lake water draining across different locales could erode and rework the local sediment. Within the model, the altitude of the bedrock beneath the ice dam in the vicinity of the Aktash settlement (**Fig. 3**) varied spatially according to the terrain from 1450 to 1250 m a.s.l., reflecting the steep bed slope at this location. The top of the ice dam was placed initially at 1650 m a.s.l. allowing for lake water to overtop the dam.

The computational mesh was created using a 1 arc-second Digital Elevation Model (DEM) dated 2015, obtained from the NASA Shuttle Radar Topography Mission (SRTM v3.0). We set the cell size to 30 m near the Sections 1–6, to 100 m in the Kuray Basin, and to 50 m along the 96 km-long Chuya Valley. Our whole system model of the megaflood from a catastrophic ice-dam failure comprises the study of the dynamics of the glacial lake, the propagation of the flood downstream of the dam, and possible mechanisms of the ice breach (i.e. instantaneous collapse of the ice dam or progressive failure with a constant ice-dam incision rate). The model was implemented in Dassflow-Shallow 2.0 (Monnier et al., 2016), which numerically solves the two-dimensional version of the unsteady shallow-water equations, also known as the Saint-Venant equations. The Manning's roughness coefficient of 0.05 s $m^{-1/3}$ was used for evaluating the hydraulic resistance (Carling et al., 2010).

Three different possible scenarios of dam failure were modelled: *i*) instantaneous removal of the ice dam; *ii*) moderate incision of the ice dam at a vertical incision rate of 42 m h^{-1}; *iii*) relatively slow incision of the ice dam at a vertical incision rate of 28 m h^{-1}. Such values of the incision rates

were the most plausible for the most significant Kuray-Chuya flood once the lake reached the surface of the ice dam at 2100 m a.s.l., and thermal erosion of the ice caused rapid growth of the sub-aerial channel in the supraglacial ice, as detailed in Bohorquez et al. (2019b). Scenario (*i*) was to simulate the sudden collapse of the ice dam due to structural failure. In contrast, the scenarios (*ii*) and (*iii*) involve degradation of the ice dam by thermal erosion as flood water passes over the ice dam. Time-series of flow parameter values, discharge, water depth, depth-averaged flow speed, flow direction, Froude number and bed shear stress, were calculated by placing virtual gauges at the studied sections. The initial motion of coarser fractions of flood sediments was evaluated in terms of the Shields number (θ), calculated using Eq. 1:

$$\theta = \frac{\tau_b}{\rho\,(S-1)g\,d} \qquad (1)$$

where τ_b is the near-bed shear stress derived from the modelling, ρ is the density of water, S is the density of quartz in water (2.65), and g is the acceleration due to gravity. The representative grain size (d) for gravels in the Kuray basin is taken as 0.035 m (Carling, 1996b). Following Carling (1996b; 1999), the critical value of θ was taken as 0.03 for the initial motion of gravels, and large gravel dunes form when $\theta > 0.11$.

4. Results and Interpretation

4.1. Geomorphology and sedimentary records

Lacustrine strandlines along the margins of the Kuray basin are clearly expressed between 2100 and 1520 m a.s.l. (Carling et al., 2011). Strandlines can be accumulative or abrasive and are almost certainly associated with both long-lived lakes and short-lived lakes separated by rapid draining events. However, to date, different suites of shorelines have not been identified that might be associated with different lake phases. Nevertheless, lacustrine deposits in the height interval of 1570–1580 m a.s.l. exposed in artificial outcrops within western part of the Kuray basin were

associated with a lake depth not less than 80 m in the center of the basin. New OSL ages (see section 4.2 “Numerical dating”) indicate that previously dated lacustrine deposits within the lake shoreline at 1650 m a.s.l. on the opposite side of the Kuray basin (Section 5, **Fig. 3**; Panin et al., 2015b) were accumulated simultaneously with the low lacustrine layer in Section 1 (**Fig. 3**). Thus, the depth of this lake was at least 170 m in the center of the basin and not less than 220 m near the mouth of the Maashey River valley, where an advanced alpine glacier could form the dam (Devyatkin, 1965). With a surface elevation at 1650 m a.s.l., the lake occupied almost the whole basin, although divided by rocky protrusions into several depressions (**Fig. 3**).

To understand the chronology and ecology of the last ice-dammed lakes in the Kuray basin, the stratigraphy of low lake strandlines at 1580, 1570 and 1525 m a.s.l. (**Fig. 3** Sections 2, 1, and 3 correspondently; **Fig. 4**) at the foot of the forebergs of the Kuray range were studied. In particular, excellent sections are exposed along a roadcut of the ‘Chuya-highway’, revealing the detailed stratigraphy of the 1570 m a.s.l. strandline of about 100 m wide, one of the lowest preserved strandlines in the basin (**Fig. 4a**). Termed Section 1 (**Fig. 3**), these 200 m-long outcrops (on both sides of the road) of lacustrine deposits and underlying gravel deposits (possibly associated with outburst floods) make this section a key for understanding the chronology, ecology and paleogeography of the last relatively large ice-dammed lakes in the Kuray basin, and clarifying the problem of correlating landforms and sediments in the basin. In addition, two shallow sections (2 and 3) of unconsolidated strandline deposits were studied at the foot of the tectonic horsebacks in the western part of the Kuray depression at 1580 and 1525 m a.s.l. near bedrock outcrops (**Fig. 4b, c**). The distance between the most remote studied sections (2 and 3), where lacustrine deposits are characterized by similar sedimentological and micropaleontological features, is about 7 km.

To identify possible sources of Tertiary organogenic material and microfauna that were redeposited into Pleistocene diluvial and lacustrine sediments a natural outcrop (**Fig. 3** Section 4, N50°15'32" E87°54'58") within the neotectonic protrusion in frontal part of the Kuray range was studied. Lake shorelines terrace the surface of this protrusion. The Oligocene-Miocene peat and

brown coal bearing deposits (Pozharisky, 1959) were exposed in a dry gully at ~1640–1650 m a.s.l., about 1.5 km northwest of Section 1. The peat horizon with visible thickness of ~0.8 m is exhumed at the bottom of the section and is draped by lacustrine loams and strongly cemented sands.

To estimate the time of final drying of the Kuray basin additionally artificial outcrops of colluvial deposits containing buried soils in a roadcut ~2.5 km upstream of the possible dam location (**Fig. 3** Section 6) were studied.

Gravel facies

Description

Sediments at Section 1 consist of pebbles, granules, grus, coarse and medium-grained sands, which form two layers of total thickness from 1.5 to 3.5–4 m (**Fig. 5a**). A basal, poorly-sorted pebble-sized gravel (D1) consisting of laminations with less than 0.1 m in thickness, fines upwards. It is unconformably overlain by thinly-laminated finer pebble and sand beds (D2) that are gently inclined towards the west, steepening locally to present as clinoforms or steeply-dipping cross-beds (**Fig. 5b**). The dip angles of the cross-beds in D2 are about 18° in the eastern part of the section. Here, the thickness of the unit is about 0.5 m. In the western part of the section, the dip angles of the cross-beds decrease to about 11°. In this (westward) direction the thickness of the D2 unit increases to more than 1.5 m together with increasing thickness of the D1 unit following the abrupt deepening of the surface of the underlying bedrocks.

In places, cut-and-fill structures truncate the otherwise largely planar bedding within D1 (**Fig. 5b**). As shown in **Fig. 5a**, many of the laminations are effectively amalgamated such that the stratification is locally indistinct. D2 in **Fig. 5a** is eroded and capped by a laminated sand bed, above which a lacustrine unit L1 overlies a thin granule bed. However, in other parts of the extensive exposures the sand bed is absent. The unconformity between the two beds, D1 and D2, undulates and is sometimes indistinct as shown in **Fig. 5a** but otherwise is distinct (**Fig. 5c**), and it can be defined by lenses of coarser gravel, including large cobbles at the base of D2.

In both D1 and D2 the direction of lamination generally is inclined westward (towards the outlet of the basin). As well as some rounded clasts, there is an abundance of sub-rounded and angular particles. Also included, in both D1 and D2, are numerous fragments of weathered particles, fragments of the weathering crust, and carbonized organic material. Pieces of organic material are spread along the bedding planes between cross-beds (**Fig. 5b**), or form clusters, including those within lenses of boulders and finer gravels between the units D1 and D2.

Gravel facies

Interpretation

The dip direction of lamination in both D1 and D2 suggests the flow was predominantly from east to west. The distinct layers represented by D1 and D2 indicate that either two flow events occurred at this location or that there was a single unsteady flow characterized by two periods of time during which the flow was competent. In either case, the second flow eroded the deposits of D1 and deposited D2 unconformably above D1. The sandy layer capping D2 indicates localized scour and the reduced flow strength at the end of a flow event. The general paucity of well-rounded clasts suggests the gravels within both units were not transported from afar, and/or the flow was not sustained for very long. This supposition is supported by the numerous carbonized and fragile weathered fragments, indicative of short-distance transport and rapid deposition. A rapid increase in velocity followed by rapid cessation of flow with decreasing water depth and a shallow flow above a bar-top is the best explanation for the character of the units. The predominance of unrounded particles in both strata and the low-angle cross-beds are reminiscent of the progradation of shallow gravel bars (Reesink, 2018), rather than the accumulation of well-rounded gravels as a result of prolonged coastal wave-cut activity of a lake with stable water level.

Sandy-clay facies

Description

At the same roadcut where we examined the D1 and D2 units, two layers of sandy-clays (L1 and L2), more sandy at the bottom, occur unconformably above the unit D2 (**Fig. 6**; see also **Fig. 5a**). Total thickness of these sandy-clay layers is the largest (up to 1.2–1.5 m) in the eastern part of the section, which is related to the eastern side of tectonic protrusion, faced to the Kuray basin. In the middle, and the highest, part of the section the layers L1 and L2 are not present. However, in the opposite roadcut (which is located practically at the same altitude) they are displayed with ~0.8 m thickness. These sandy-clay deposits are present again in the western margin of the Section 1 (total thickness reaches 0.5–0.6 m), and they gradually disappear westward. In this western part of the section (which is related to the western side of tectonic protrusion, faced to the tributary valley), lacustrine deposits are displaced down the slope and are covered with a cross-bedded diluvium. Thickness of diluvium also increases westward (from 0.2 up to ~1.5 m) together with the thinning of the lacustrine deposits. The horizons L1 and L2 are separated by a thin (0.05–0.15 m) sandy cross-bedded interlayer. Thickness of this interlayer significantly increases up to ~1 m in the eastern part of the section, where it hosts lenses of fine gravels. Convolutions and numerous crack displacements are present mainly in the eastern part of the Section 1 (**Fig. 7**), where the surface of the bedrock inclines towards the center of the basin. Deposits have been subject to rupture, after emplacement and consolidation, with displacements along cracks in the lacustrine loams as well as in overlying fossil soil. In places, there is a distinct soft-sediment convolution of L2 into L1 disrupting the intervening interlayer (**Fig. 6b** and **7a**). Loams of both L1 and L2 layers exhibit large schlieren texture indicating that they were affected by freezing after accumulation.

Two additional exposures (Sections 2 and 3; **Fig. 3**) provide additional information. Section 2 constitutes a horizon, up to 0.6 m-thick, of brownish (whitish in dry state) loams exposed under alluvial-diluvial (?) deposits and contemporary soil found along the lake strandlines (**Fig. 4b** and **8**). The horizon is deformed by cracks and broken into separate blocks, some of which are shifted down the slope up to 3 m. These loams exhibit large schlieren texture.

Section 3 is represented by two outcrops located 20 m from each other with an altitudinal difference of about 2 m (**Fig. 4c** and **9**). Neogene (?) clays are exhumed in the downslope 2 m high outcrop (**Fig. 9a**). These clays were redeposited by the winnowing activity of Pleistocene lakes, and form the basal deposits (I) of the sedimentation sequence of the upslope 2.5 m high outcrop (**Fig. 9b**). This basal unit is represented by thin interlaying of “chocolate” and yellow-brownish layers, and is covered by a horizon (II) of wavy-laminated medium sands with interlayers and lenses of brownish loams with a total thickness of about 20–25 cm. Lacustrine deposits (III) above are about 1.2 m thick and consist of up to four layers (each <30 cm thick) of brownish (whitish in a dry state) loams, with interbedded layers of loams with fine sands and grus, and layers of medium sands. On top of the section, there are reworked pedogenetic sandy loam slope deposits (IV) with inclusions of grus, and fluvially-derived granules and pebbles. The total thickness of the surface deposit is about 0.6 m with humus-rich pedogenesis extending to a depth of 0.3 m.

Deposits in Section 3 are disturbed and displaced along the numerous cracks, most likely of seismic origin, formed after their dewatering and consolidation. Both redeposited Neogene (?) clays and Pleistocene loams have a schlieren texture.

Sandy-clay facies

Interpretation

The L1 unit at Section 1 is interpreted as lacustrine sediments deposited under shallow water inundation of the D2 unit leading to erosion of the D2 unit to produce the unconformity between the beds. As the strandline marks the margin of the lake, at this level the water could not have been deep (<100 m). A significant drawdown of lake level occurred at least once as indicated from the scour and sandy interlayer between L1 and L2, with the lake deepening subsequently to form L2. The origin of the convolution and crack displacements is less clear. The convolution might be due to significant wave action leading to slumping of unconsolidated fine lacustrine deposits. Alternatively, strong seismic activity in the region (Rogozhin et al., 2008; Nepop and Agatova,

2018) could have affected the sediments soon after deposition whilst sediments remain water-saturated. Consolidation and dewatering would have prevented the forming of seismites if earthquake activity occurred significantly later than when the sediments were first deposited, and caused the forming of cracks. Some cracks in the eastern part of Section 1 cut through buried soils dated 3.6 ka cal BP (see section 4.2 “Numerical dating” below).

As in the case of the Section 1 the sediment assembly at Sections 2 and 3 represent thin lacustrine deposits deformed along the strandline level by a rapid lake drawdown. Although thin, the sandy-grus-gravel may correlate with the better-defined D2 gravel at Section 1 which is associated with a flood across the strandline surface, possibly related to a rapid lake drainage. Numerical dating is necessary to confirm this suggestion.

4.2. Numerical dating

The new ages presented in this study were analyzed together with consideration of previously published ^{14}C and OSL dates (**Tab. 1** and **2**; **Fig. 10**). For OSL dating at Section 1, a sample was obtained from a sandy bed at the top of D2 (just below L1) and another sample was taken from a sandy lens within the convoluted interface between L1 and L2 in the eastern part of the section (**Fig. 6b**). Three more samples in different parts of the section were collected for radiocarbon dating. The generalized scheme of Section 1 with locations of all collected samples is shown in **Fig. 9**. Additionally, organic material was sampled from a peaty layer from undivided Oligocene-Miocene deposits in Section 4 (**Fig. 3**). In the western part of the Kuray basin, 3 km from the probable ice-dam location, a section of colluvial deposits (**Fig. 11)** was studied in a trench 30 m above the modern Chuya river at 1475 m a.s.l. (Section 6 in **Fig. 3**). In this section a horizon of fossil soil covers the ancient talus fan and is buried by a 10-m-thick deposit of light brown sandy loam with slightly inclined interbeds of grus, gravel, and boulders. Another horizon of fossil soil on the top this sequence is buried by younger colluvium with the contemporary soil.

The OSL ages of 19.0 ± 1.1 ka (GdTL-2590) and 16.0 ± 1.7 ka (GdTL-2591) for sandy layers above and below the lacustrine L1 unit, together with the radiocarbon age of 3640 ± 270 cal BP (SOAN-9496) for fossil soil above the lacustrine deposits at Section 1 indicate a lake formation in Sartan time (MIS-2). The OSL ages bracket the formation age for the lower lacustrine horizon between ~19 and 16 ka. The abrupt drop of the lake level and accumulation of a sandy layer between the lacustrine silts occurred ~16 ka, before the lake level rose again.

The time of accumulation of the upper cross-bedded layer (D2) is characterized by the OSL age of 19.0 ± 1.1 ka (GdTL-2590) from the sandy layer at the top of D2. Four ^{14}C ages for the organic material from the D2 unit (**Fig. 12**), which is associated with an outburst flood, range between ~25.0-39.4 ka cal BP. Additionally, radiocarbon dating from the lower diluvial unit (D1) returned younger and stratigraphically inconsistent ages of about 14.5 and 8.2 ka cal BP. It should be noted that these ^{14}C dates do not indicate the true age for the organic inclusions, as well as the age of enclosing sediments. The biological composition of several studied fragments provide evidence for the possible redeposition of Tertiary peats and brown coals as a result of winnowing activity of the Pleistocene ice-dammed lakes (Agatova et al., 2019b). One of the nearest locations of such old carbon deposits are the Oligocene-Miocene brown coal-bearing deposits exposed in Section 4, about 1.5 km from Section 1. Brown coal-bearing deposits in Section 4 as well as studied inclusion of organic matter in low diluvial unit in Section 1 contain fragments of *Sparganium* and *Potamogeton*, which indicates possible redeposition of Tertiary material during cataclysmic outburst floods. A ^{14}C age of 39.5 ± 2.1 ka cal BP (IGAN-4811; **Tab. 1**, Section 4 in **Fig. 3**) for organic material from Tertiary peat horizon at the bottom of the section is near the limits of the radiocarbon dating method. Generally, infiltration of young carbon into an ancient organic material explains the obtained apparent ^{14}C ages of redeposited organic fragments (Section 1) and peat layers *in situ* (Section 4). This issue of contamination is a quite common problem for the Quaternary geochronology of the SE Altai where surface exposures of coal-bearing Tertiary, Middle and Upper Carboniferous, and Lower Jurassic deposits were affected by exogenous processes, including fluvial

activity within the Pleistocene basins, and were later redeposited as inclusions of old organic material into younger sediments of different genesis (Agatova et al., 2017a, 2019b).

The final draining of ice-dammed lakes in the Kuray and Chuya basins is associated with the final glacial degradation that took place before ~9.9 ka cal BP and further subaerial sedimentation occurred at ~9.9–8.2 ka cal BP (**Tab. 1, Fig. 13**), as well as the formation of a local, landslide-dammed lake above diluvial deposits at around 9.7 ka cal BP (Butvilovsky, 1993). Radiocarbon ages of organic material in lacustrine deposits at 1750 m a.s.l. within the high-elevation Yeshtykkel plateau could indicate the formation of a local lake at around 12.8–12.7 ka cal BP (Butvilovsky, 1993; Rusanov and Orlova, 2013). More accurately, the termination of the lake period within the Kuray and Chuya basins is evident from the ages of fossil soils in the immediate vicinity of the possible dam locations, around 9.9 and 8.2 ka cal BP (**Tab. 1, Fig. 13**).

4.3. Micropaleontological estimations

To make stratigraphic and paleoecological reconstructions micropaleontological analysis was utilized. Freshwater ostracods were recovered from all sections (1–4) with lacustrine deposits and the most detailed study was conducted at Section 1. Here, the ostracods were studied in three profiles – in the western, central, and eastern parts of the section. Since lacustrine horizons in the central part of Section 1 are completely eroded, the ostracods were studied on the opposite side of the roadcut in the ‘Chuya-highway’, down the slope, where total thickness of L1 and L2 layers reached 0.8 m. Generally, in places where eroded sediments were exposed to the surface and affected by pedogenesis no ostracods were detected due to their dissolution with humic acids. In addition to ostracods, a few fragments of rootlets of aquatic plants and fish scales were recovered. An undisturbed fish scale was also discovered in lacustrine deposits in Section 3.

The same association of ostracods, consisting mainly of two species: *Leucocythere* sp.1 and *Leucocythere* sp.2, was detected in all studied samples from sections 1 to 4. In some samples we also detected *Leucocythere dorsotuberosa* Huang, *Leucocytherella sinensis* Huang in small

amounts, and just occasionally only in the eastern part of Section 1, affected by convolutions, there were single determinations of *Eucypris* sp., *Candona* sp., *Cyprinotus* sp., *Ilyocypris* sp. (**Fig. 14**). The last species differ sharply in their appearance compared with the other species. They have yellow color, are rounded, often broken, and filled with dense sediments. These characteristics indicate that they were redeposited. The redeposited shells are presented in the bottom of the lower lacustrine horizon (L1 in Section 1) and appeared again immediately above and below the sandy layer that separates the lacustrine horizons. This sandy layer indicates the abrupt dropping of the lake level. The redeposited ostracods (*Limnocythere sp., Cyprinotus sp., Eucypris sp.*) along with autochthon species were also detected in Section 3. Generally, ostracod redeposition could be controlled by erosion (winnowing) of Tertiary deposits, which are exposed on the surface in this part of the Kuray basin. Intensification of winnowing occurs during filling and abrupt draining of a lake.

The two most common species of the autochthon ostracod association (L. sp.1 and L. sp.2) are defined in the open nomenclature, but they are not new species. They were found outside the Russian Altai – in mountain lakes within the Tibetan Plateau, where they are present both in living and fossil form (Mischke et al., 2010a, 2010b; Zhang et al., 2013; Yan and Wünnemann, 2014). Until now, they were considered as endemics, but our discovery argues that the distribution of these ostracod species is not limited only to Tibet. Because these species of ostracod found in the Altai are currently extant, their ecological preferences are well studied (Mischke et al., 2010a, 2010b; Zhang et al., 2013; Yan and Wünnemann, 2014). *Leucocythere* sp.1. lives in shallow water depths (0.2–15 m), and is adapted to hard and unstable biotopes. In contrast, *Leucocythere* sp.2. prefers deeper lakes (>15 m with an optimum depth of about 30 m; Yan and Wünnemann, 2014). *Leucocythere dorsotuberosa* also prefers deep waters (maximum population densities are reported at depths more than 26 m), generally settling in the profundal parts of lakes, but can be also detected in shallow waters (Akita et al., 2016). All these species are alpine forms, which prefer to inhabit periglacial cold and deep lakes. It should be noted that in the Russian Altai these freshwater species

co-existed in the Kuray ice-dammed lake, while in the Tibetan Plateau each species was found in different reservoirs.

Leucocythere sp.1 and *Leucocythere* sp.2 are euryhaline species that endure a wide range of salinity, from 0 to 40 ‰ (Yan and Wünnemann, 2014). In the Tibetan associations, they are found together with a pronounced halophile - *Eucypris mareotica*, although the quantitative curve of these species has an inverse relation. *Leucocythere* sp.1 reaches a maximum population density in waters with a salinity of about 5 ‰ (Zhang et al., 2013).

4.4. X-ray diffractometry and IR spectroscopy

X-ray diffraction and IR spectroscopic analyses of the Late Pleistocene lacustrine deposits from two horizons in Section 1 and the deposits in Section 3 revealed a predominance of terrigenous minerals. Quartz, feldspar, and layered silicates (chlorite and mica) prevailed, while mixed-layer illite-smectite, kaolinite, and amphibole were detected in minor amount. Authigenic minerals are presented as calcite (in both sections) and more rarely as gypsum (horizon 140–145 cm in Section 3). The diffraction spectra of some samples that characterize the mineral composition of the lacustrine deposits are shown in **Fig. 15**.

The mineral composition of the sediments indicates that:

- Presence of well-crystallized mica and chlorite in lacustrine deposits indicates cold, dry conditions at the time of their formation, as well as a predominance of physical weathering of rocks within the denudation area (Singer, 1984; Joussain et al., 2016).
- There is a greater increase of carbonate concentration in lacustrine sediments of the upper horizon (L2) than the low horizon (L1) in Section 1 (**Fig. 15 a, c**), which can be explained either by intensification of the chemogenic mineral formation or by an increase of carbonate influx from the lake shores. Both factors indicate a more shallow lake in comparison with that where a low horizon (L1) was accumulated. Absence of correlation between the number

of ostracods and the presence of calcite in sediments may indicate that the accumulation of calcite is not associated with biogenic carbonate formation.

- Similar mineral compositions were observed in the lacustrine deposits in sections 1 and 3 (**Fig. 15**). Together with the similar set of autochthon Pleistocene ostracods it is evidence for the same paleoenvironmental conditions and possible synchronous sedimentation in these two sections. OSL dating of deposits in Section 3 may clarify this issue.

4.5. Lake drainage modelling

Time series of the flow depth, depth-averaged flow velocity, non-dimensional bed shear stress and Froude number were calculated at the location of Section 1 from the draining of a 1650-m a.s.l. lake after three different scenarios of ice-dam breach: (*i*) instantaneous, (*ii*) moderate incision and (*iii*) slow incision. Peak discharges integrated across the whole basin width for a transect across Section 1 were: (*i*) ~2 × 10^6 m^3 s^{-1}, (*ii*) 1 × 10^6 m^3 s^{-1} and (*iii*) 0.7 × 10^6 m^3 s^{-1}, as shown in **Fig. 16a**. It took ~55 hours to drain the lake completely, but for scenario (*i*) little water remained in the basin after 20 hours and after 30 hours in scenarios (*ii*) and (*iii*). However, Section 1 was already dry within 4 hours after the initial dam breach (**Fig. 16b**). The calculated shear stress of the flow at the location of Section 1 shows that only the flood triggered from scenario (*i*) was able to mobilize gravel-sized particles and the scenarios (*ii*) and (*iii*) were not considered for further analysis.

Time-series of flood parameters for the Section 1 outcrop are plotted as a thick solid curve in **Figs. 16c–e**. After the breaching of the ice dam, water level fell steadily (**Fig. 16b**); the flow direction initially was north-of-west as water moved towards the basin outlet, but then stabilized and flowed away from the strandline towards the basin center to the south (**Fig. 16c**). The Froude number increased steadily during the initial draining to Fr = 0.093 at ~17 min after the breach but then declined to a low value until it peaked again (Fr = 0.134) ~4 hours after the breach, during the shallow and rapid runoff at the end of the draining (**Fig. 16d**). We note that the Froude number remained sub-critical at all times such that supercritical bedforms such as antidunes could not have

developed, although the development of dunes cannot be precluded. In contrast, the shear stress peaked only once during the initial draining of the lake. For a short time, the Shields parameter exceeded a threshold of 0.03 for gravel entrainment (**Fig. 16e**), and the lake water draining across the locale could erode and rework the local sediment. This result is consistent with our interpretation of the gravel facies, which shows that the gravel within both units was not transported far, and the competent flow was not sustained for very long. According to the bedform stability diagram by Bohorquez et al. (2019a), the Shields parameter and the grain roughness relative to flow depth achieved the threshold values of 0.07 and 4×10^{-4}, respectively, for large dune formations, but the short duration of the sediment transport period prevented their full development (Carling 1996b, 1999).

In Sections 3 and 6, the flow lasted longer (i.e., 8 h 30 min and 30 h, respectively), while it ceased just in 36 and 93 minutes in Sections 2 and 4 (**Fig. 16b**). The longer or shorter duration of the flow at each location is consistent with the deeper or shallower flow before the dam break, which can also be observed in the map of the maximum depth in the Kuray lake (**Fig. 17a**). The competence to mobilize sediments in such locations is assured by the high speeds developing there, i.e. 1.9–5.6 m s^{-1} (**Fig. 17b**), that provoked maximum Froude numbers of 0.06–0.22 (**Fig. 17c**) and peak Shields values of 0.03–0.25 (**Fig. 17d**). Interestingly, locations 1, 3 and 4 lie in regions with local maxima of velocity and bed shear stress nearby (see **Figs. 17b** and **17d**), dropping the Shields parameter below the threshold for sediment motion a few kilometers away. In accord with the results for Section 1, the duration of the erosion stage in the rest of the locations was too short for the development of bedforms.

Lastly, the maps of maximum values of the Froude and the Shields numbers also serve to illuminate the capability of the current flood to reactivate the dune fields of Aktru and Kuray (dashed areas in **Fig. 17**). We found Froude numbers in the range of 0.1–0.2 (**Fig. 17c**) which are characteristic of dunes, but the Shields parameter was too low ($\theta < 0.02$ in **Fig. 17d**) to erode and transport gravels over the dune fields (Carling et al. 2016).

5. Discussion

The main problem of paleoecological reconstructions on the basis of ostracod analysis in the SE Altai is the lack of information and descriptions of these hydrobionts in the region. Recent publications on ostracods in the Russian Altai reported predominantly Miocene-Pliocene associations and indicated some of their common features with Caucasian associations (Teterina, 2012; Rusanov et al., 2017). Holocene complexes, described in some sections in the region, are represented by typical West Siberian species that are widespread within the Siberian plain (Rusanov and Teterina, 2018). The Pleistocene of the Russian Altai is the least characterized period in terms of micropaleontological data, and the presented results significantly enriches this dataset. In general, the study of ostracods associations in mountainous environments is complicated by fragmentation of their habitats due to vertical zoning and a high degree of endemism due to geographical isolation of populations.

The gravel units D1 and D2 indicate either a single two-pulsed flood or two separate floods crossing the location of Section 1. Unit D1 is largely horizontally bedded and might be related to strong water currents flowing across the location of Section 1 from east to west. However, the absence of any indication of dune morphology at the top of D2 indicates that the D2 unit was not formed by the migration of gravel dunes. The presence of a single bed (D2) characterized by low-angle clinoforms that only locally steepen to form cross-beds near the angle of repose can be used to argue that the gravel dunes are not likely responsible for the sedimentary structure of unit D2. Rather, the structure has more affinity with the migration of a unit bar front (Reesink, 2018) from east to west as the lake drained. Unit bars commonly form in relatively shallow water and they must have pertained close to a lake shoreline. The thickness of inclined bed-sets in such simple bars often directly reflects the height of the bedform (Bridge and Lunt, 2008; Reesink et al., 2015), so it is evident that the bar front was no more than a couple of meters high at most, and often less, as is evident from the thickness (0.5 to 1.5m) of the D2 cross-bedded unit.

Recognizing sedimentation patterns and numerical dating of deposits in key Section 1 is of vital importance for making chronological and paleogeographical reconstructions of the last ice-dammed lake in the region. Vysotsky (2009) described the sedimentary records in this location and reported a single radiocarbon date (**Tab. 1**). He also gives more detailed description of sediments uncovered in a nearby quarry (0.5 km eastward of Section 1). The altitude of the quarry is ~20 m lower than Section 1 and a larger outcrop (about 20 m of uncovered loose sediments) allowed tracing of the sedimentation history for a deeper reservoir. At the bottom of the section, Vysotsky (2009) reports partly winnowed slope deposits exposed above yellow-greenish siltstone, which covers the bedrock protrusion at the foot of the Kuray range. These slope deposits are cut by a nonconformity caused by fluvial erosion and overlain by three packages of gravel deposits, which are either normal small-scale fluvial (Vysotsky, 2009) or diluvial (as it was described by Vysotsky in the catalog of radiocarbon dates; Rusanov and Orlova, 2013). The gravels in turn are capped by whitish loams at the surface. However, no genetic interpretation for the loams was provided in these two publications. The upper package of fluvial (or diluvial) deposits is characterized by crossbedding. The upper part of the section reported by Vysotsky (2009) appears to correlate with Section 1 of this study, which is interpreted here to be diluvial.

Earlier Efimtcev (1968, p. 58) described deposits in Section 1 as an “ancient alluvial cone” and taking into account their geomorphological position and sedimentation patterns correlated them with deposits of the Inya sequences within Chuya and Katun River valleys (which were also interpreted by Efimtcev as “ancient alluvium”). Today the Inya sequence is generally associated with deposits of cataclysmic outburst floods (e.g., Herget, 2005; Zolnikov and Mistrukov, 2008; Panin et al., 2015a; Zolnikov et al., 2016; Krivonogov et al., 2017). Krivonogov et al. (2017) characterized the deposits in Section 1 as “weakly rounded gravels which were probably accumulated by moving waters of the Chuya-Kuray paleolake during the megaflood discharge” without any additional genetic interpretations.

In contrast, Zolnikov (2011) supposed an alluvial origin for these cross-bedded gravels and sands, as well as their stratigraphic location above lacustrine deposits and proposed a more ancient age for the last ice-dammed lake formation in Kuray basin (older than MIS-2; Zolnikov, 2011; or during MIS-4; Zolnikov et al., 2016). The chronological reconstructions in Zolnikov (2011) are based on a single ^{14}C age of 24975 ± 575 cal BP (SOAN 4971) originally reported by Vysotsky (2009) for a "wood fragment" collected from the cross-bedded grus-sandy-gravel layer (D2) in Section 1. Numerous pieces of organic material that often look similar to charcoal can be found in both D1 and D2 layers from this section and they were later radiocarbon dated to ~8.2–39.4 ka cal BP (**Tab. 1, Fig. 12**). Organic material we collected indicates that at least some of these pieces could be redeposited fragments of Tertiary peats. As shown in this study, the presence of a fish scale and ostracods indicate that the sediments in the upper part of Section 1 are lacustrine, not subaerial. To argue for an older than MIS-2 age for the timing of the last ice-dammed lake formation in the Kuray basin, Zolnikov and Mistrukov (2008) also used a ^{14}C age of 32.2 ± 2.6 ka cal BP (Beta 137035 UM993; Okishev and Borodavko, 2001) and wrongly cited it as the timing for development of a "subaerial cover complex". Originally, this ^{14}C age was reported as the age for a remnant of peaty vegetation in coastal lacustrine sediments, which corresponds to the timing of lake terrace formation at ~1860 m a.s.l. (Okishev and Borodavko, 2001, p. 24–25). However, numerous radiocarbon dates of fossil soils, buried peats, fragments of charcoals and vegetation remnants from subaerial deposits within the Chuya-Kuray intermontane depressions returned the oldest ^{14}C ages of ~8.2–13.8 ka cal BP (**Fig. 13;** Agatova et al., 2016). Similar results were reported by Butvilovsky (1993). It may be concluded that the Holocene ages may apply for all the studied subaerial sediments and align more likely with the MIS-2 estimates for the timing of the draining of the last ice-dammed lakes, than MIS-4 as was suggested by Zolnikov (2011) and Zolnikov et al. (2016).

We noted the common problem of mixing older carbon-rich material into Pleistocene and Holocene sediments (Agatova et al., 2017a, 2019b). The Tertiary peats exposed in Section 4 were reworked by Pleistocene ice-dammed lakes and the associated outburst floods. Penetrating of the

“young” carbon into ancient organic material, and its presence in a unique (for each sample) ratio should be stated. Today such contamination cannot be eliminated completely utilizing standard pre-treatment techniques. Thus, obtained radiocarbon dates often contradict the stratigraphic order, paleontological and mineralogical characteristics of deposits, as well as their position in the geomorphic system (Agatova et al., 2017a, 2019b). Generally, apparent ^{14}C ages from the region, often near the upper time limit of the dating technique, are not reliable age markers and should be accepted with caution only if they have independent control from other proxy age data.

An OSL age of 18.2 ± 1.1 ka for a mixed-sized sandy layer from the depth of 1.2 m in one of the low lake terraces at 1650 m a.s.l. in Kuray basin (**Fig. 3**, Section 5) was reported by Panin et al., (2015b). The considerable width (about 30 m) of the strandline, its cross profile (deepening of the surface to the back of the terrace, associated with presence of berm and runnel), which is typical for wave-generated coastal bars, and the sediment composition (prevailing of mixed-sized sands and fine gravels) argue for prolonged existence of such a lake with a stable water level. These results together with our new data are evidence that the lake filled the Kuray basin at least up to 1650 m a.s.l. at ~16–19 ka.

The presence of dropstones in the lake basin is related to Quaternary glaciers extending into the lake and calving icebergs (Devyatkin, 1965; Reuther et al., 2006; Rusanov, 2008). Based on ^{10}Be ages for dropstones within the area of investigations (including those found on the Kuray basin floor), the last outburst flood from the Kuray-Chuya ice-dammed lakes occurred at 18.7 ± 1.6 ka (as previously reported ^{10}Be data by Reuther et al. (2006) was recalculated by Gribenski et al. (2016)). Reuther et al. (2006) associated the cataclysmic draining event with the maximal filling of the paleolake up to ~2100 m a.s.l. Our study indicates that the last ice-dammed lake in the Kuray basin was not the largest, and filled the depression up to at least 1650 m a.s.l. Nevertheless, such lakes inundated the basin (most likely repeatedly) and prevented the dropstones and moraine boulders to be fully exposed to cosmic rays since their initial deposition; thus, the calculated ^{10}Be ages may

have been underestimated. Such a scenario was previously discussed by Reuther et al. (2006), and possible underestimation of ^{10}Be ages was first suggested by Gribenski et al. (2016).

Today the time of the final drying of Kuray basin is still unknown. Earlier, on the basis of an uncalibrated radiocarbon date 10845 ± 80 (SOAN 2346, presented by Butvilovsky (1993), **Tab. 1**, **Fig. 13**) Rudoy (2002) suggested drying of the basin later than ~11 ka ago. The sample SOAN 2346 represents detritus collected from lacustrine loams on the western bank of the Dzhangyskel lake (1750 m a.s.l.) within the high-elevation Yeshtykkel plateau (Butvilovsky, 1993; Rusanov and Orlova, 2013), which is furthermore not the lowest part of the Kuray Basin (**Fig. 3**). Two more radiocarbon dates of similar and older ages are also reported for sediments of this lake (SOAN 1645, Utc 8470, **Tab. 1, Fig. 13**). The presence of organic detritus and fragments of wood indicate climatic amelioration and degradation of MIS-2 glaciers within the Yeshtykkel plateau by ~15.6 ka cal BP (Blyakharchuk et al., 2008). Thus, the mentioned radiocarbon dates indicate lacustrine sedimentation in this location and should not be interpreted as drying of this part of the basin, where the modern but small Dzhangyskel lake still exists. Moreover, the water level ~1650 m a.s.l. of the last ice-dammed lake (as argued in this paper) is 100 m lower than the Yeshtykkel plateau. The large redeposited fragment of travertine in diluvium at 1600 m a.s.l. within the southwestern part of the Kuray basin (**Fig. 2**) was dated applying the radiocarbon technique (after Butvilovsky in Rusanov and Orlova, 2013). The reported age of 21010 ± 1320 cal BP is similar to the obtained OSL age of 19.0 ± 1.1 ka of the upper diluvial unit in Section 1. Nevertheless, the ^{14}C age for the travertine should be used cautiously as a geochronological marker of the last cataclysmic outburst flood because a source of carbon for the travertine was not studied and it is not *in situ*. In contrast to such uncertainty, our results suggest that final drying of the Kuray basin occurred before ~9.9 ka cal BP as indicated by the age of fossil soil located at 1475 m a.s.l. (just 25 m above the Chuya River) in the western part of the basin (location 6 in **Fig. 3**, **Fig. 11**).

The question of the possible ice dam location is still open. There are no direct numerical ages, necessary to reliably determine the timing and extent of the last advance of the Maashey glacier

during MIS-2 (**Fig. 3**). Reconstructed parameters of the last ice-dammed lake in the Kuray basin suggests that an ice mass slightly higher than 200 m near the mouth of the Maashey river valley would have been enough to provide an ice-dam for the 1650 m a.s.l-level lake. Therefore, there is no necessity to reconstruct a powerful and vast ice sheet glaciation over the Kuray range with further formation of >350 m thick outlet glaciers near the Aktash settlement for MIS-2. Such an advance of the Maashey glacier during the Last Glaciation was earlier suggested by Devyatkin (1965, fig. 45). Further investigations and solving the problem of chronology and magnitudes of Pleistocene glaciations in the SE Altai will clarify this issue.

One of the paleogeographical problems in the region is the chronological correlation of low lake strandlines and gravel dunes within the Kuray depression (Panin, 2013; Panin et al., 2015b). In particular, giant gravel dunes are found at several locations in both the Chuya and Kuray basins and have been related to disturbance of the lake bed during drainage (Carling, 1996a, b; Bohorquez et al., 2016). Giant gravel dunes (with no lacustrine deposits on their surface) are evidence for the cataclysmic draining of the last major lake. In contrast, the low lacustrine strandlines indicate that the last ice-dammed lake in the Kuray basin was not the largest one, and, therefore, its drainage probably could hardly produce such prominent landforms as giant gravel dunes. Geomorphic and sedimentary features of the lowest strandlines in the basin argue for prolonged existence of that last lake (Panin, 2013; Panin et al., 2015b). Carling et al. (2016) visualized the distinct layers within the giant gravel dunes using ground-penetrating radar. Recent lake draining modelling (Bohorquez et al., 2019b) indicates that drainage of the largest lake was very unsteady, producing at least three periods of dune migration during the single event. Earlier Carling et al. (2016) argued that the dunes could have been formed during multiple phases of a single flood, or the layers could have been superimposed sediments from three or more separate floods. In the latter case, the lake was assumed to have refilled on a number of occasions with the dunes being reactivated by each draining event.

Although the last lake drainage event described in this paper was not powerful enough to form large dunes, our new data suggest that both low lake strandlines and giant gravel dunes in the Kuray

basin could be related to the last ice-dammed lake and its draining. If dunes formed by an earlier lake drainage event were present at the time of this final draining, probably, only the last stage of gravel dune migration as recorded by Carling et al. (2016) is correlated with the late flood event. The flood simulations produced by Bohorquez et al. (2019b) indicate that drainage of the last substantial lake was very unsteady, producing at least three short periods of dune migration during the single event each of which would progress dunes (Carling et al. 2016). The dunes could have been already in the basin due to an earlier flood and were reactivated. Although the threshold of dune migration (θ = 0.03, according to Carling (1996b; 1999)) was not exceeded for long, the bed shear stresses was of sufficient magnitude and duration to entrain any finer lacustrine deposits which might blanket the older dunes and evacuate this material from the basin.

Suggested scenario:

Ice-dammed lakes could repeatedly occupy the Kuray basin during MIS-2 although the size of these lakes remains uncertain until high-level strandlines are dated. An outburst flood from such a reservoir occurred earlier than or around 19 ka and caused the accumulation of the horizontally and cross-bedded grus-sand-gravel deposits with lenses of boulders within the western part of the Kuray depression. Between 16 and 19 ka the last low-altitude ice-dammed lake with the water level of at least 1650 m a.s.l. was formed. The depth of this last reservoir was at least 170 m in the central part of the basin and about 220 m near the mouth of the Maashey valley, where the advanced Maashey glacier could have served as a dam. Around 16 ka the water level fell, and the lake did not recover above the depth of at least 80 m. The timing of the final draining of this last ice-dammed lake is not clearly defined. However, there was no lake in the Kuray basin by 9.9 ka cal BP. The last flood event probably reactivated gravel dunes formed by an earlier flood event. Downstream of the dam, the final outburst flood passed along the river valleys, which had been already developed by more ancient cataclysmic floods, and thus, it did not significantly affect the topography, compared to the erosion by more powerful ancient floods.

It should be also mentioned that the ice-dammed lakes formation and their cataclysmic draining influenced the human occupation of the Kuray basin and the main river valleys during the late Paleolithic, which is broadly dated in the Russian Altai as 60–10 ka BP (Derevianko and Shunkov, 2004). Reconstructing the last cataclysmic outburst floods along the Chuya and Katun river valleys during the cool substages of MIS-5, Zolnikov et al. (2016) suggested favorable living conditions for ancient people since 90 ka. Today 20 late Paleolithic sites have been discovered around the periphery of the Chuya basin. At the same time, only four of them are stratified. All these stratified finds, including the most ancient artifacts showing the Levallois reduction technique, are located above the highest lacustrine strandlines at 2100 m a.s.l. (**Fig. 13**), and, therefore, cannot be used to clarify the chronology of ice-dammed lakes (Agatova and Nepop, 2017b). Below 2100 m a.s.l. only surface finds (i.e., artifacts found on the surface beyond the cultural layer, which was accumulated at a site as a result of ancient human activity) were discovered, most of which expressed clear signs of surface displacement. Despite the occurrence of numerous traces of redeposition of artifacts, the current location of the lowermost Paleolithic sites does not contradict the possible existence of paleolakes at an altitude of 1770 m a.s.l and below. Only a single stone implement, which was redeposited into lacustrine sediments of ~5.5 ka cal BP (Butvilovsky, 1993), was found within the Kuray basin. The inundation of the Kuray basin by ice-dammed lakes during MIS-2 could explain the continued absence of Paleolithic surface finds within the floor of the basin.

6. Conclusion

The results of multidisciplinary investigations, including geomorphological and sedimentological analyses, micropaleontological and mineralogical characteristics of lacustrine deposits, numerical simulation of flood, as well as new OSL and radiocarbon dates are presented. These new data, together with consideration of previously published information, indicate that repeated ice-dammed lakes formed within the Kuray depression (SE Altai) during MIS-2. The last

lake existed ~16–19 ka with the maximum water filling the central part of the basin to a depth of 170 m and to a depth of ~220 m near the glacier dam.

The mineralogical data indicate that the lower horizon of the lacustrine deposits in the western part of the Kuray basin was accumulated under a deeper lake than the higher lacustrine horizon. Thus, after an abrupt dropping of the lake level (which is also evident within the sedimentological and micropaleontological record) at about 16 ka, determined from OSL dating, the lake never recovered its former depth. The Kuray basin was finally dry by 9.9 ka cal BP.

Analysis of ostracods in lacustrine deposits, as well as organic inclusions in flood deposits, provide evidence for the erosion and redepositing of Tertiary lacustrine and boggy sediments during the period of the late Pleistocene ice-dammed lakes. The redeposited ostracod shells are presented at the bottom of the lower lacustrine horizon, whereas higher in the section, their number drops sharply. Redeposited ostracods appear again during the abrupt dropping of the lake level and the accumulation of a sandy layer between lacustrine horizons at ~16 ka. Species typical of the Chinese association of ostracods from the Tibetan Plateau - *Leucocythere* sp.1, *Leucocythere* sp.2, *Leucocythere dorsotuberosa* Huang, and *Leucocytherella sinensis* Huang, were detected for the first time among autochthonous ostracods in the Kuray basin. All these species are characteristic of Late Pleistocene-Holocene deep cold freshwater periglacial lakes. The new data are in agreement with previously published micropaleontological data from the Tibetan Plateau and geochronological data from the SE Altai.

The new data contribute to the probable chronological correlation of the low lake strandlines in the Kuray basin with landforms associated with cataclysmic outburst floods. The size of the last Late Pleistocene ice-dammed lake in the Kuray basin was enough to trigger an outburst flood with estimated peak discharge of ~2×10^6 m^3 s^{-1}. High speeds of the water flow, 1.9–5.6 m s^{-1}, calculated maximum Froude numbers of 0.06–0.22, and peak Shields values of 0.03–0.25 indicate the competence to mobilize sediments, and, probably, to mobilize the last generation of gravel dunes.

Acknowledgment

Dr. Uspenskaya (RRIVG RAAS, Moscow) is kindly thanked for establishing the biological composition of sediments, including the Tertiary peat, and Dr. Vysotsky (IGM SBRAS, Novosibirsk) for providing two radiocarbon dates. We appreciate valuable comments of two anonymous reviewers that helped to improve style and content of the manuscript. Professor Juergen Herget is kindly thanked for his careful editorial handling.

The study was supported by State Assignment of IGM SO RAN and partly funded by Russian Foundation for Basic Researches (grant 18-05-00998). We also benefited from the funds of the projects EX-AQUA (1623P) "Palaeohydrological Extreme Events - evidence and archives", sustained by INQUA TERPRO. The flood modelling contribution by Bohorquez was supported by the Spanish Ministry of Science, Innovation and Universities (MICINN/FEDER, UE) under Grant SEDRETO CGL2015-70736-R.

References

Agatova, A.R., 2005. Geomorphologic mapping of the Chagan-Uzun river basin: a reference for reconstructing history of Pleistocene glaciations in the Southeastern Altai. Stratigraphy and Geological Correlation. 13(6), 656-666.

Agatova, A.R., Nepop, R.K., Bronnikova, M.A., Slyusarenko, I.Yu., Orlova, L.A., 2016. Human occupation of South Eastern Altai highlands (Russia) in the context of environmental changes. Archaeological and Anthropological Sciences 8, 419-440.

Agatova, A.R., Nepop, R.K., 2017a. Pleistocene glaciations of the SE Altai, Russia, based on geomorphological data and absolute dating of glacial deposits in Chagan reference section. Geochronometria. 44, 49-65.

Agatova, A.R., Nepop, R.K., 2017b. Connection of the Late Paleolithic Archaeological Sites of the Chuya Depression with Geological Evidence of Existence of the Late Pleistocene Ice-Dammed Lakes. Stratigraphy and Geological Correlation. 25(4), 463-478.

Agatova, A.R., Nepop, R.K., Rudaya, N.A., Khazina, I.V., Zhdanova, A.N., Bronnikova, M.A., Uspenskaya, O.N., Zazovskaya, E.P., Ovchinnikov, I.Y., Panov, V.S., Shurygin, B.N., 2017a. Discovery of Upper Oligocene–Lower Miocene brown coal deposits (Kosh-Agach formation) in the Dzhazator River valley (Southeastern Russian Altai): Neotectonic and paleogeographical aspects. Doklady Earth Sciences. 475(2), 854-857.

Agatova, A.R., Nepop, R.K., Slyusarenko, I.Y., 2017b. Archaeological Sites as Markers of Hydrosystem Transformation in the Kurai and Chuya Basins, Southeastern Altai, in the Late Pleistocene and Holocene. Summary of Findings and Paleogeographic Reconstructions. Archaeology, Ethnology & Anthropology of Eurasia. 45(1), 25-35.

Agatova, A.R., Nepop, R.K., Khazin, L.B., Zhdanova, A.N., Uspenskaya, O.N., Ovchinnikov, I.Yu., Moska, P., 2019a. New chronological, paleontological and geochemical data on developing of ice-dammed lakes in Kurai basin (southeastern part of Russian Altai) during the end of Late Pleistocene. Doklady Earth Sciences 488(1), 1134-1136.

Agatova, A.R., Nepop, R.K., Zazovskaya, E.P., Ovchinnikov, I.Yu., Moska, P., 2019b. Problems of developing the Pleistocene radiocarbon chronology within high mountain terraines by the example of Russian Altai. Radiocarbon.

Aitken, M.J., 1998. An Introduction to Optical Dating. The Dating of Quaternary Sediments by the Use of Photon-stimulated Luminescence. Oxford University Press, Oxford.

Akita, L.G., Frenzel, P., Wang, J., Börner, N., Peng, P., 2016. Spatial distribution and ecology of the Recent Ostracoda from Tangra Yumco and adjacent waters on the southern Tibetan Plateau: A key to palaeoenvironmental reconstruction. Limnologica. 59, 21-43.

Arslanov, A.A., 1987. Radiocarbon: Geochemistry and Geochronology. Leningrad State University Press, Leningrad (in Russian).

Bailagasov, L.B., Bailagasova, I.L., 2008. To the issue of the size and water level of the Uimon paleolake. Nature resources of Gorny Altai 1(9), 53-59 (in Russian).

Baker, V.R., Benito, G., Rudoy, A.N., 1993. Palaeohydrology of Late Pleistocene superflooding, Altay Mountains, Siberia. Science 259, 348-350.

Berger, G.W., 2010. An alternate form of probability- distribution plot for De values. Antient TL. 28, 11-22.

Blyakharchuk, T., Wright, H., Borodavko, P., Knaap, W.O., van der Ammann, B., 2008. The role of pingos in the development of the Dzhangyskol lakeepingo complex, central Altai Mountains, southern Siberia. Palaeogeography Palaeoclimatology Palaeoecology. 257, 404-420.

Bohner, J., 2006. General climatic controls and topoclimatic variations in Central and High Asia. Boreas. 35(2), 279-295.

Bohorquez, P., Carling, P. A., Herget, J., 2016. Dynamic simulation of catastrophic late Pleistocene glacial-lake drainage, Altai Mountains, central Asia. International Geology Review 58(14), 1795-1817.

Bohorquez, P., Cañada Pereira, P., Jimenez-Ruiz, P.J., del Moral-Erencia, J.D., 2019a.The fascination of a shallow-water model for the formation of megaflood-scale dunes and antidunes. Earth-Sci. Rev. 193, 91–108. https://doi.org/10.1016/j.earscirev.2019.03.021.

Bohorquez, P., Jimenez-Ruiz, P.J., Carling, P.A., 2019b. Revisiting the dynamics of catastrophic late Pleistocene glacial-lake drainage, Altai Mountains, central Asia. Earth-Science Reviews, 197, 102892.

Bøtter-Jensen, L., Bulur, E., Duller, G.A.T., Murray, A.S., 2000. Advances in luminescence instrument systems. Radiation Measurements. 32, 523-528.

Bridge, J.S., Lunt, I.A., 2006. Depositional models of braided rivers. Braided Rivers: Process, Deposits, Ecology and Management, Int. Assoc. Sedimentol. Spec. Publ., 36, 11-55.

Butvilovsky, V.V., 1985. Cataclysmic water discharge from ice-dammed lakes in the SE Altai and their surface effects. Russian Geomorphology. 1, 65-74 (in Russian).

Butvilovsky, V.V., 1986. Cataclysmic outburst floods from periglacial lakes in the SE Altai. Russian Geology and Geophysics. 4, 27-36 (in Russian).

Butvilovsky, V.V., 1993. Paleogeography of the Last Glaciation and the Holocene of Altai: a catastrophic-events model. Tomsk University Press, Tomsk (in Russian).

Butvilovsky, V.V., Panychev, V.A., Lammert, A.K., 1991. Age, morphology and history of development of the last glaciation of Eastern Altai. Materials of Glaciological Investigations. 73, 36-43 (in Russian).

Butvilovsky, V.V., Butvilovskaya, T.V., Avvakumov, A.E., 1996. Geomorphological mapping of Gorny Altai. Report of the regional geological group on the scientific researches carried out in 1989-1996. Novokuznetck: State registration number 13-89-106/1 (in Russian).

Butvilovsky, V.V., Prehtel, N., 2000. Peculiarities of the last ice age in the basin of Koksa and the upper reaches of Katun. Modern Problems of Geography and Environmental Management 2, 31-47 (in Russian).

Carling, P.A., 1996a. Morphology, sedimentology and palaeohydraulic significance of large gravel dunes, Altai Mountains, Siberia. Sedimentology 43(4), 647-664.

Carling, P.A., 1996b. A preliminary palaeohydraulic model applied to late Quaternary gravel dunes: Altai Mountains, Siberia. Geological Society, London, Special Publications, 115(1), 165-179.

Carling, P.A., 1999. Subaqueous gravel dunes. Journal of Sedimentary Research. 69, 534.

Carling, P.A., 2013. Freshwater megaflood sedimentation: What can we learn about generic processes? Earth-Science Reviews. 125, 87-113.

Carling, P.A., Kirkbride, A.D., Parnachev, S., Borodavko, P.S., Berger, G.W., 2002. Late Quaternary catastrophic flooding in the Altai Mountains of south–central Siberia: A synoptic overview and introduction to flood deposit sedimentology. In: Martini, I.P., Baker, V.R., Garzón, G. (Eds.), Flood and Megaflood Processes and De-posits: Recent and Ancient Examples. International Association of Sedimentologists, Special Publication 32, pp. 17-35.

Carling, P., Villanueva, I., Herget, J., Wright, N., Borodavko, P., Morvan, H., 2010. Unsteady 1D and 2D hydraulic models with ice dam break for Quaternary megaflood, Altai Mountains, southern Siberia. Global and Planetary Change 70(1), 24-34.

Carling, P.A., Knaapen, M., Borodavko, P., Herget, J., Koptev, I., Huggenberger, P., Parnachev, S., 2011. Palaeoshorelines of glacial lake Kuray-Chuja, south-central Siberia: form, sediments and process. Geological Society, London, Special Publications 354(1), 111-128.

Carling, P.A., Bristow, C.S., Litvinov, A.S., 2016. Ground-penetrating radar stratigraphy and dynamics of megaflood gravel dunes. Journal of the Geological Society. 173(3), 550-559.

Derevyanko, A.P., Molodin, V.I., 2000. Phenomenon of Altai Mummies. Publishing House of the Institute of Archaeology and Ethnography SB RAS, Novosibirsk (in Russian).

Derevianko, A.P., Shunkov, M.V., 2004. Formation of the Upper Paleolithic traditions in the Altai. Archaeology, Ethnology & Anthropology of Eurasia. 3 (19), 12-40.

Devyatkin, E.V., 1965. Cenozoic deposits and neotectonics of Southeastern Altai. Moscow, USSR Academy of Science (In Russian).

Efimtcev N.A., 1968. On the latest regional foreland basins (by the example of Gorny Altai), in Florensov N.A. (Ed.) Problems of geomorphology and neotectonics of orogenic regions of Siberia and the Far East. Science, Novosibirsk, pp. 54-64 (in Russian).

El Ouahabi, M., Hubert-Ferrari, A., Fagel, N., 2017. Lacustrine clay mineral assemblages as a proxy for land-use and climate changes over the last 4 kyr: The Amik Lake case study, Southern Turkey. Quaternary International. 438, 15-29.

Fagel, N., Thamó-Bózsó, E., Heime, B., 2007. Mineralogical signatures of Lake Baikal sediments: Sources of sediment supplies through Late Quaternary. Sedimentary Geology. 194, 37–59.

Galbraith, R.F., Roberts, R.G., Laslett, G.M., Yoshida, H., Olley, J.M., 1999. Optical dating of single and multiple grains of quartz from Jinminum Rock Shelter, Northern 12 Australia. Part I, experimental design and statistical models. Archaeometry. 41, 1835- 1857.

Galakhov, V.P., Samoilova, S.Y., Shevchenko, A.A., Sheremetov, R.T., 2015. Fluctuation of Maly Aktru Glacier (Russian Altai) for the period of instrumental observations from 1952 to 2013. Earth Cryosphere. 2, 70-75.

Ganiushkin, D., Chistyakov, K., Kunaeva, E., 2015. Fluctuation of glaciers in the southeast Russian Altai and northwest Mongolia Mountains since the Little Ice Age maximum. Environmental Earth Sciences. 3(74), 1883-1904.

Gribenski, N., Jansson, K.N., Lukas, S., Stroeven, A.P., Harbor, J.M., Blomdin, R., Ivanov, M.N., Heyman, J., Petrakov, D.A., Rudoy, A., Clifton, T., Lifton, N.A., Caffee, M.W., 2016. Complex patterns of glacier advances during the late glacial in the Chagan Uzun Valley, Russian Altai. Quaternary Science Reviews. 149, 288-305.

Groswald, M.G., Rudoy, A.N., 1996. Quaternary ice-dammed lakes in mountains of Siberia. Proceedings of Russian Academy of Science. 6, 112-126 (in Russian).

Guerin, G., Mercier, N., Adamiec, G., 2011. Dose-rate conversion factors: update. Ancient TL 29, 5-8.

Herget, J., 2005. Reconstruction of Pleistocene ice-dammed lake outburst floods in the Altai Mountains, Siberia. Geological Society of America Special Papers 386.

Herget, J., Carling, P., Agatova, A., Batbaatar, J., Borodavko, P., Gillespie, A., Nepop, R., 2017. Comment on Gribenski, N. et al., 2016. Complex patterns of glacier advances during the late glacial in the Chagan Uzun Valley, Russian Altai. Quaternary Science Reviews. 149, 288-305.

Herget, J., Agatova, A., Carling, P., Nepop, R., 2020. Altai megafloods – the temporal context. Earth-Science Reviews. 200, 102995.

Joussain, R., Colin, C., Liu, Z., Meynadier, L., Fournier, L., Fauquembergue, K., Zaragosi, S., Schmidt, F., Rojas, V., Bassinot, F., 2016. Climatic control of sediment transport from the Himalayas to the proximal NE Bengal Fan during the last glacial-interglacial cycle. Quaternary Science Reviews. 148, 1-16.

Korde, N.V., 1960. Biostratigraphy and Typology of Russian Gyttja. USSR Academy of Science, Moscow (in Russian).

Krivonogov, S., Zolnikov, I., Novikov, I., Deev, E., 2017. Giant glaciogenic floods in Altai: geomorphological, geological and hydrological aspects. Guidebook for field excursion at the 14th International Workshop on Present Earth Surface Processes and Long-term Environmental Changes in East Eurasia. NSU Publisher, Novosibirsk.

Lehmkuhl, F., Zander, A., Frechen, M., 2007. Luminescence chronology of fluvial and aeolian deposits in the Russian Altai (Southern Siberia). Quaternary Geochronology. 2, 195-201.

Li, M., Kang, S., Zhu, L., You, Q., Zhang, Q., Wang, J., 2008. Mineralogy and geochemistry of lacustrine sediments in Nam Co, Tibet. Quaternary International. 187, 105-116.

Mikhailov, N.N., Redkin, A.T., 1997. Limnic-glacial complexes of Ukok plateau. Geography and environmental management of Siberia. 2, 62-70 (in Russian).

Mischke, S., Aichner, B., Diekmann, B., Herzschuh, U, Plessen, B., Wünnemann, B., Zhang, C., 2010a. Ostracods and stable isotopes of a late glacial and Holocene lake record from the NE Tibetan Plateau. Chemical Geology. 276, 95-103.

Mischke, S., Bößneck, U., Diekmann, B., Herzschuh, U., Jin, H., Kramer, A., Wünnemann, B., Zhang, C., 2010b. Quantitative relationship between water-depth and sub-fossil ostracod assemblages in Lake Donggi Cona, Qinghai Province, China. Journal of Paleolimnology. 43, 589-608.Murray, A.S., Wintle, A.G., 2000. Luminescence dating of quartz using an improved singlealiquot regenerative-dose protocol. Radiation Measurements. 32, 57–73.

Monnier, J., Couderc, F., Dartus, D., Larnier, K., Madec, R., Vila, J.P., 2016. Inverse algorithms for 2D shallow water equations in presence of wet dry fronts: Application to flood plain dynamics. Adv. Water Resour. 97, 11–24.

Moore, D.M., Reynolds, R.C.J., 1997. X-ray Diffraction and the Identification and Analysis of Clay Minerals. Oxford University Press, Oxford-New York.

Murray, A.S., Wintle, A.G., 2000. Luminescence dating of quartz using an improved single-aliquot regenerative-dose protocol. Radiation measurements, 32(1), 57–73.

Narozny, Yu.K., Osipov, A.V., 1999. Oroclimatic conditions of the Central Altai glaciations. Regional Research of Russia. 131(3), 49–57 (in Russian).

Nepop, R.K., Agatova, A.R., 2018. Recurrence interval of strong earthquakes in the SE Altai, Russia revealed by tree-ring analysis and radiocarbon dating. Geochronometria. 454, 20-33.

Novikov, I.S., Parnachev, S.V., 2000. Morphotectonics of late quaternary lakes in river valleys and intermountain troughs of southeastern Altai. Russian Geology and Geophysics. 41(2), 227-238 (in Russian).

Okishev, P.A., 1982. The dynamics of glaciation in Altai during the Late Pleistocene and Holocene. Tomsk University Press, Tomsk (in Russian).

Okishev, P.A., Borodavko, P.S., 2001. New materials on the history of the Chuya-Kurai limnosystem. Issues of Geography of Siberia 24, 18-27 (in Russian).

Panin, A.V., 2013. Self-organization of fluvial systems and fluvial catastrophes in the Altai. Russian Geomorphology. 4, 80-85 (in Russian).

Panin, A., Baryshnikov, G., 2015. Composition and geochronology of the low (Saldzhar) terrace at the Chuya River confluence. In: Baryshnikov, G., A. Agatova, P. Carling, J. Herget, A. Panin, G. Adamiec & R. Nepop (eds.): Russian Altai in the last Pleistocene and the Holocene - geomorphological catastrophes and landscape rebound (fieldtrip guide). Barnaul, 68-72.

Panin, A., Adamiec, G., Baryshnikov, G., 2015a. General description and absolute geochronology of the Bolshoi Yaloman exposure. In: Baryshnikov, G., Agatova, A., Carling, P., Herget, J., Panin, A., Adamiec, G., Nepop, R. (Eds.), Russian Altai in the last Pleistocene and the Holocene - geomorphological catastrophes and landscape rebound (fieldtrip guide). Barnaul, 41-47.

Panin, A., Baryshnikov, G., Adamiec, G., 2015b. Kuray strandlines - supplement. In: Baryshnikov, G., Agatova, A., Carling, P., Herget, J., Panin, A., Adamiec, G., Nepop, R. (Eds.), Russian Altai in the last Pleistocene and the Holocene - geomorphological catastrophes and landscape rebound (fieldtrip guide). Barnaul, 106-107.

Pattyn F., De Smedt B., Van Huele W., Agatova A., Mistrukov A., Decleir H., 2003. Ice dynamics and basal properties of Sofiyskiy Glacier, Altai Mountains, Russia, based on DGPS and radio-echo sounding surveys. Annals of Glaciology 37, 286-292.

Pozdnyakov, A.V., Khon, A.V., 2001. About the genesis of “giant ripple bars” in Kurai basin, Gorny Altai. Bulletin of Tomsk State University. 274, 24-33 (in Russian).

Pozharisky, I.F., (editor), 1959. Geological map: M-45-XVI. USSR Geological Map. Series Gorny Altai, scale: 1: 200000. Aerogeological Trust.

Prescott, J.R., Stephan, L.G., 1982. The contribution of cosmic radiation to the environmental dose for thermoluminescence dating. Latitude, altitude and depth dependencies. TLS II-1, pp.16-25.

Reesink, A.J.H., 2018. Interpretation of cross strata formed by unit bars. Int. Assoc. Sedimentol. Spec. Publ., 48, 173-200.

Reesink, A.J.H., Parsons, D.R., Van den Berg, J., Amsler, M.L., Best, J.L., Hardy, R.J., Lane, S.N., Orfeo, O., Szupiany, R., 2015. Extremes in dune preservation; controls on the completeness of fluvial deposits. Earth-Sci. Rev. 150, 652-665.

Reimer, P.J., Bard, E., Bayliss, A., Beck, J.W., Blackwell, P.G., Bronk Ramsey, C., Buck, C.E., Cheng, H., Edwards, R.L., Friedrich, M., Grootes, P.M., Guilderson, T.P., Haflidason, H., Hajdas, I., Hatté, C., Heaton, T.J., Hogg, A.G., Hughen, K.A., Kaiser, K.F., Kromer, B., Manning, S.W., Niu, M., Reimer, R.W., Richards, D.A., Scott, E.M., Southon, J.R., Turney, C.S.M., Van der Plicht, J., 2013. IntCal13 and MARINE13 radiocarbon age calibration curves 0-50000 years calBP. Radiocarbon 55(4). 1869-1887.

Reuther, A., Herget, J., Ivy-Ochs, S., Borodavko, P., Kubik, P.W., Heine, K., 2006. Constraining the timing of the most recent cataclysmic flood event from ice-dammed lakes in the Russian Altai-Mountains, Siberia, using cosmogenic in situ 10Be. Geology 34, 913-916.

Rogozhin, E.A., Ovsyuchenko, A.N., Marakhanov, A.V., 2008. Major earthquakes of the southern Gorny Altai in the Holocene. Izvestiya Physics of the Solid Earth. 44(6), 469-486.

Rudoy, A.N., 1988. Regime of ice-dammed lakes in the intermontane basins of Southern Siberia. Materials of Glaciological Investigations. 61, 36-44 (in Russian).

Rudoy, A.N., 2002. Glacier-Dammed Lakes and geological work of glacial superfloods in the Late Pleistocene, Southern Siberia, Altai Mountains. Quaternary International 87(1), 119-140.

Rudoy, A.N., 2005. Giant Current Ripples. Tomsk, Tomsk State University (in Russian).

Rudoy, A.N., Baker, V.R., 1993. Sedimentary effects of cataclysmic late Pleistocene glacial outburst flooding, Altay Moutains, Siberia. Sedimentary Geology. 85, 53-62.

Rudoy, A.N., Rusanov G., 2010. The last glaciation in north-western Altai Mountains. Tomsk. (in Russian).

Rusanov, G.G., 2008. The maximal level of the Chuya ice-dammed lake in the Altai Mountains Russian Geomorfology. 1, 65-71 (in Russian).

Rusanov, G.G., Orlova, L.A., 2013. Radiocarbon Dates (SOAN) of Gorny Altai and Altai Foreplain. “Biya” Publisher, Bijsk (in Russian).

Rusanov, G.G., Deev, E.V., Zolnikov, I.D., Khazin, L.B., Khazina, I.V., Kuzmina, O.B., 2017. Reference section of Neogene-Quaternary deposits in the Uimon Basin (Gorny Altai). Russian Geology and Geophysics. 58(8), 973-983.

Rusanov, G.G., Teterina, I.I., 2018. Lakes and landscape-climate features of the Altai highlands and middle altitude areas in the second half of the Holocene. Siberian State Technology University, Novokuznetsk (in Russian).

Sheinkman, V.S., 1990. Pleistocene glaciations of mountains of Siberia: analysis and new data. Materials of Glaciological Investigations 69, 78-85 (in Russian).

Sheinkman, V.S., 2011. Glaciation in the High Mountains of Siberia, in: Ehlers, J., P.L. Gibbard, P.D. Hughes (Eds.), Quaternary glaciations - extent and chronolgy, a closer look. Amsterdam, 883-907.

Singer, A., 1984. The paleoclimatic interpretation of clay minerals in sediments – a review. Earth-Science Reviews. 21 (4), 251-293.

Skripkin, V., Kovaliukh, N., 1997. Recent Developments in the Procedures Used at the SSCER Laboratory for the Routine Preparation of Lithium Carbide. Radiocarbon 40(1). 211-214.

Solotchina, E.P., Prokopenko, A.A., Vasilevsky, A.N., Gavshin, V.M., Kuzmin, M.I., Williams, D.F., 2002. Simulation of XRD patterns as an optimal technique for studying glacial and interglacial clay mineral associations in bottom sediments of Lake Baikal. Clay minerals. 37(1), 105-119.

Solotchina, E.P., Prokopenko, A.A., Kuzmin, M.I., Solotchin, P.A., Zhdanova, A.N., 2009. Climate signals in sediment mineralogy of Lake Baikal and Lake Hovsgol during the LGM-Holocene

transition and the 1-Ma carbonate record from the HDP-04 drill core. Quaternary International. 205(1-2), 38-52.

Svitoch, A.A., Boyarskaya, T.D., Voskresenskaya, T.N., Glushakova, I.I., Evseev, A.V., Kursalova, V.I., Parmonova, N.N., Faustov, S.S., Khorev, V.S., 1978. The sections of the latest deposits of Altai. MSU Publisher, Moscow (in Russian).

Teterina, I.I., 2012. New species of Pliocene ostracods of the Southeast Altai. Bulletin of Tomsk State University. 364, 223-226 (in Russian).

Uspenskaya, O.N., 1986. General patterns of formation and development of lakes, in Treshnikov, A.F., Kvasov, V.A, Rumjancev, V.A. (Eds.), Methods of studying the history of lakes. Nauka, Leningrad, pp 146-151 (in Russian).

Vysotsky, E.M., 2009. The age of relief forming of weelhead part of Kurai depression (Gorny Altai). Proceedings of the VI All-Russian Quaternary conference “Fundamental Problems of Quaternary: Results and Trends of Future Researches”, SB RAS Publisher, Novosibirsk. P. 137-138 (in Russian).

Weatherbase, Kosh-Agach, Russia. http://www.weatherbase.com/weather/weather.php3?s=95263 (accessed 15 December 2019).

Walker, J.R., 1993. An introduction to computer modeling of X-ray powder diffraction patterns of clay minerals: a guided tour to NEWMOD. In: Reynolds, R. C. J., Walker, J.R. (Eds.), CMS Workshop Lectures, Computer Applications to X-ray Diffraction Analysis of Clay Minerals. Clay Minerals Society, Boulder, 2-17.

Yan, D., Wünnemann, B., 2014. Late Quaternary water depth changes in Hala Lake, northeastern Tibetan Plateau, derived from ostracod assemblages and sediment properties in multiple sediment records. Quaternary Science Reviews. 95, 95-114.

Zhang, W., Mischke, S., Zhang, C., Gao, D., Fan, R., 2013. Ostracod distribution and habitat relationships in the Kunlun Mountains, northern Tibetan Plateau. Quaternary International. 313-314, 38-46.

Zolnikov, I.D., 2011. Role of glaciations and glacial megafloods in geological structure of the Neopleistocene sedimentary complexes in Gorny Altai and Altai foreplain. Doctoral Thesis. Novosibirsk: OIT IPGG SB RAS, 35p. (in Russian).

Zolnikov, I.D., Mistrukov, A.A., 2008. Quaternary deposits and relief of the Chuya and Katun valleys. Parallel, Novosibirsk (in Russian).

Zolnikov, I.D., Deev, E.V., Kotler, S.A., Rusanov, G.G., Nazarov, D.V., 2016. New results of OSL dating of Quaternary sediments in the Upper Katun'valley (Gorny Altai) and adjacent area. Russian Geology and Geophysics 57(6), 933-943.

Zykin, V.S., Zykina, V.S., Smolyaninova, L.G., 2016. New data on the most ancient early Quaternary glaciation in Gorny Altai. Doklady Earth Sciences 466(1), 20-23.

Figure captions

Fig. 1. Location of the SE Altai and adjacent areas within the Altai-Sayan mountain province. The acronyms indicate the names of the intermountain depressions: U- Uimon, K- Kuray, Ch- Chuya; Dzh- Dzhulukul; B- Bertek.

Fig. 2. Schematic map of sedimentary filling of the Kuray depression and landforms associated with cataclysmic draining of ice-dammed lakes suggested by Butvilovsky (1993) based upon drilling reports of Kuray geological exploration expedition and the summary of the geological surveys of the Joint Stock Company «Zapsibgeolsyomka». Genesis of sediments is marked by letters: g- glacial; d- diluvial; l- lacustrine; a- alluvial. The age of the deposits is indicated as □- Paleogene; N- Neogene; Q- Quaternary; *S*- Last Glacial (Sartan); *H*- Holocene.

Fig. 3. The extent of the last ice-dammed lake in the Kuray basin. The sections numbered from 1 to 6 are discussed in the text.

Fig. 4. Geomorphological position of the studied sections. Outcrop locations are presented in Fig. 3. Field car in (a) and (c) is 2 m high and 4 m long. (a) Section 1: West-east stretch of sediments along the roadcut in a strandline at altitude of ~1570 m a.s.l. (N50°09'10" E87°58'50"). Dotted squares indicate the positions of units discussed in text and in Figs. 5 and 6. (b) View to southwest along the 'Chuya-highway'. North Chuya range in the background. Section 2 is in the roadcut outcrop below lowest strandline at altitude of ~1580 m a.s.l. (N50°14'50" E87°50'20"). (c) Section 3 near Kuray settlement at ~1525 m a.s.l. (N50°14'070" E87°56''40 ").

Fig. 5. Gravel facies presented in Section 1. See Fig. 4a for outcrop locations. The spade in (a) is 0.85 m long. (a) Oblique view of the sediments showing the relationship of the units D1, D2, and

L1. (b) Closer view of the small-scale planar cross-beds (occasionally are slightly sigmoidal in form) with numerous inclusions of organic material, occur towards the top of D2. The sand bed at top right is the same sand bed seen in (a). (c) The relationship between units D1 and D2 at ~80-m-thick exposure, westward from a location pictured in (a). Here the upwardly fining bedding is thicker and rhythmic than within D1. The clinoforms within D2 have variable inclination and often are cross-cutting. Sandy top sets occur on several clinoform surfaces, as with the example just right of the D2 symbol. Slope-wash colluvium caps the sequence top-left, as L1 is absent at this exposure. Concentrations of large well-rounded cobbles along the unconformity between D1 and D2 form occasional coarse gravel lenses in shallow scour holes. The gravels sometimes include small boulders, as seen in the displaced example in the foreground.

Fig. 6. Sandy-clay facies presented in Section 1. See Fig. 4a for outcrop locations. (a) A distinct two-layered sandy-clay unit occurs above the D2 gravel and is capped by colluvium with fossil and contemporary soils on the top. The distinction between the two is evident to the right of the image where the base of L2 forms a shadowed overhang. (b) Convolution of L2 with L1 is shown along the interface between the two beds.

Fig. 7. Convolutions and crack displacements in the eastern part of Section 1. See Fig. 4a for outcrop locations. Outcrop on panel (a) is an eastern part of outcrop, shown on Fig. 6b.

Fig. 8. Deformed horizon of lacustrine loams covered by slope deposits with inclusions of grus, gravel, pebbles and modern soil exposed in Section 2. Arrows indicate the broken and displaced downslope parts of the soil.

Fig. 9. Lacustrine deposits exhumed in Section 3. The spade in (a) is 1.2 m long and sections on the measuring tape in (b) are 0.1 m long. (a) Neogene (?) clays in the downslope outcrop and (b)

sedimentation sequence in the upslope outcrop: I - basal pack of redeposited Neogene clays; II - horizon of wavy-laminated fine sands with interlayers and lenses of gravels, grus, and inclusions of weathering crust; III - unit of lacustrine deposits with sandy interlayers; IV - grayish carbonate silt reworked by soil processes with inclusions of grus, pebbles, and single boulders.

Fig. 10. Distribution of equivalent dose measurements (black dots with 1σ standard error bars) and the relative probability density plots of the data (Berger, 2010) for the OSL samples. The sample GdTL-2590 was collected at the top of D2; GdTL-2591 was collected between L1 and L2.

Fig. 11. Geomorphological position of Section 6 (1475 m a.s.l. N50°15'10" E87°42'30") and the radiocarbon ages for the fossil soils. The height of people in the photo are about 180 cm; field car measures 2 × 2 × 4 m. Mouth of the Maashey valley, where a possible glacier dam could be located 2.5 km westward, is shown with an arrow. Stripes indicate Pleistocene lacustrine deposits preserved around the bedrock protrusions; white dashed line with arrows indicates former river bed and flow direction of the former Chuya river; red ovals indicate burial mounds associated with the Pazyryk culture of Scythian epoch (late 9^{th}–3^{rd} centuries BC).

Fig. 12. Generalized scheme of units in Section 1 and the numerical ages. Genesis of sediments is indicated with letters: Ae- aeolian; L- lacustrine; D- diluvial.

Fig. 13. The oldest radiocarbon ages (cal BP) associated with the termination of lake period in the Chuya-Kuray basins and the locations of Paleolithic sites in the region. The ages denoted with asterisks indicate samples collected from lacustrine deposits; other samples were taken from subaerial deposits (see also **Tab. 1** for details).

Fig. 14. Ostracods found in the lacustrine deposits in Sections 1–4. A – *Leucocythere* sp.1. Left valve, female. B – *Leucocythere* sp.1. Left valve, male. C – *Leucocythere* sp.2. Right valve, female. D, E, and F – Ostracoda spp. Redeposited valves. The length of the white bars is 0.5 mm.

Fig. 15. X-ray diffraction spectra of lacustrine deposits. Section 1: (a) the upper L2, and (c) lower L1 layers; Section 3: (b) from the upper (100–105 cm) and (d) lower (140–145 cm) parts.

Fig. 16. Results of the numerical simulation of flood events. (a) Flood hydrographs at the location of Section 1 from a lake with water level at ~1650 m a.s.l. simulated with three different dam failure scenarios: instantaneous failure, moderate and slow incision. (b) Water depth as a function of time at several sections due to instantaneous draining. Panels (c)–(e) show the velocity magnitude, Froude number and Shields parameter as a function of time at Section 1 due to instantaneous draining. The inset in (c) represents the velocity direction where the values of 180, 270, and 360 degrees correspond to the South, West, and North, respectively. The horizontal pecked lines in (e) are the thresholds for gravel motion, $\theta = 0.03$, and dune formation, $\theta = 0.11$ (Carling 1996b, 1999).

Fig. 17. Flooding maps of maximum values in the Kuray lake during the instantaneous draining: (a) water depth, (b) velocity, (c) Shields and (d) Froude number.


85°
95°
86°
88°
90°
50°
45°
49°
Elevation (m a.s.l.)
0 - 200
200 - 500
500 - 1000
1000 - 2000
2000 - 3000
3000 - 4000
4000 - 6000
SAYAN
ALTAI
RUSSIA
Katun river
Chuya river
Chulyshman plateau
Dzh
U
K
Kuray range
Chikhachev range
North Chuya range
Katun range
South Chuya range
Ch
Ukok plateau
Sailugem range
KAZAKHSTAN
B
MONGOLIA
CHINA
0
40 km
N

Figure 1

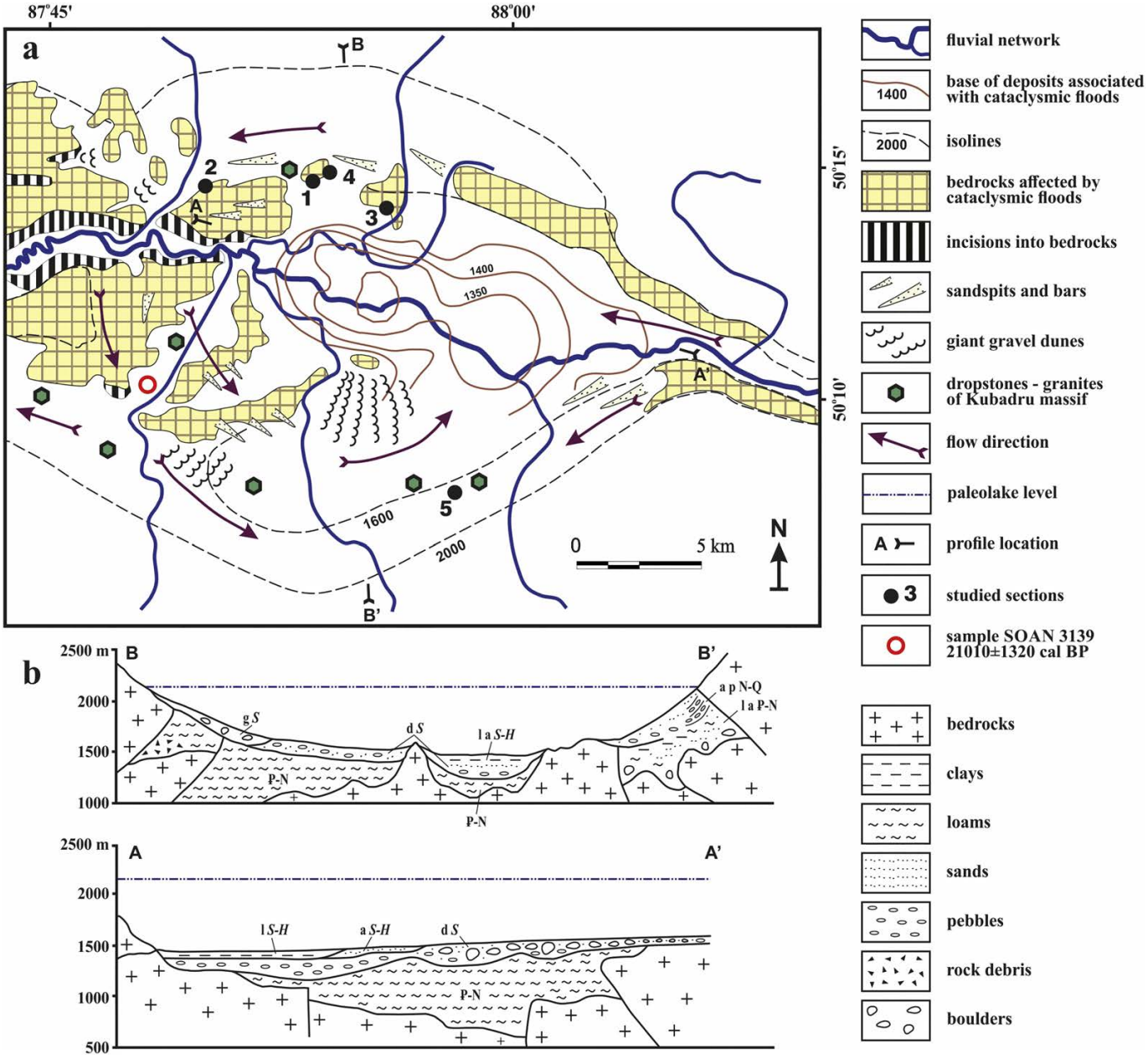
87°45'
88°00'
50°15'
50°10'
a
B
A
1
2
3
4
5
1400
1350
1600
2000
A'
B'
0
5 km
N
fluvial network
base of deposits associated with cataclysmic floods
1400
isolines
2000
bedrocks affected by cataclysmic floods
incisions into bedrocks
sandspits and bars
giant gravel dunes
dropstones - granites of Kubadru massif
flow direction
paleolake level
A
profile location
3
studied sections
sample SOAN 3139
21010±1320 cal BP
b
2500 m
2000
1500
1000
B
B'
g S
d S
l a S-H
P-N
a p N-Q
l a P-N
2500 m
500
A
A'
l S-H
a S-H
d S
bedrocks
clays
loams
sands
pebbles
rock debris
boulders

Figure 2

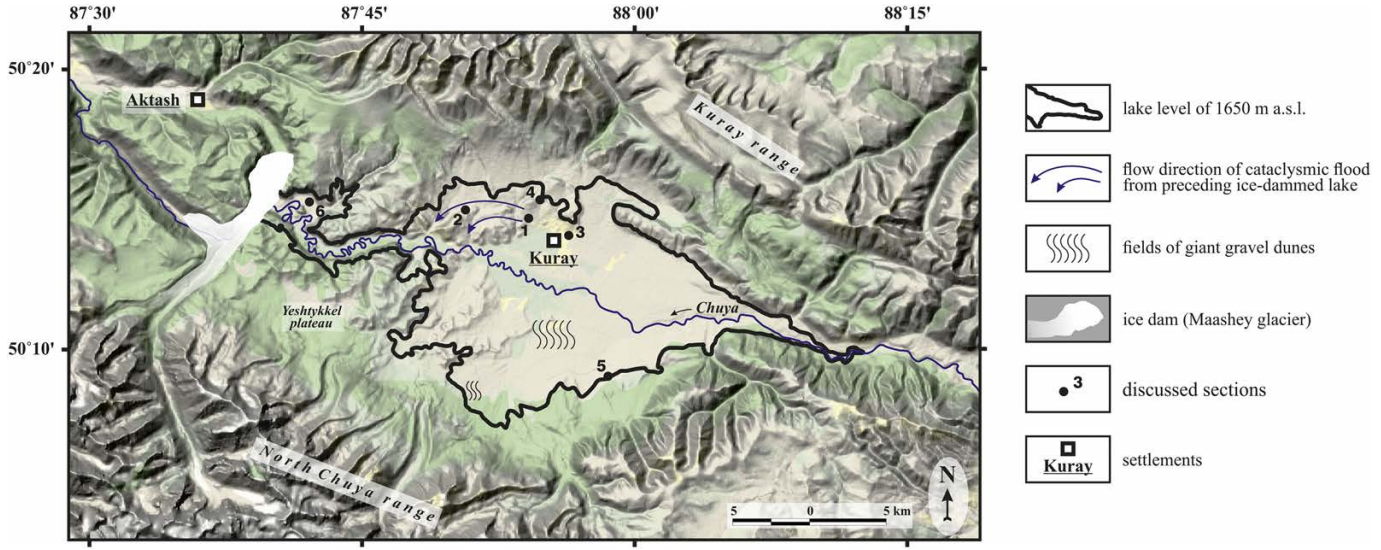
87°30'
87°45'
88°00'
88°15'
50°20'
50°10'
Aktash
Kuray range
Kuray
Yeshtykkel plateau
Chuya
North Chuya range
1
2
3
4
5
6
5 0 5 km
N
lake level of 1650 m a.s.l.
flow direction of cataclysmic flood from preceding ice-dammed lake
fields of giant gravel dunes
ice dam (Maashey glacier)
discussed sections
settlements

Figure 3

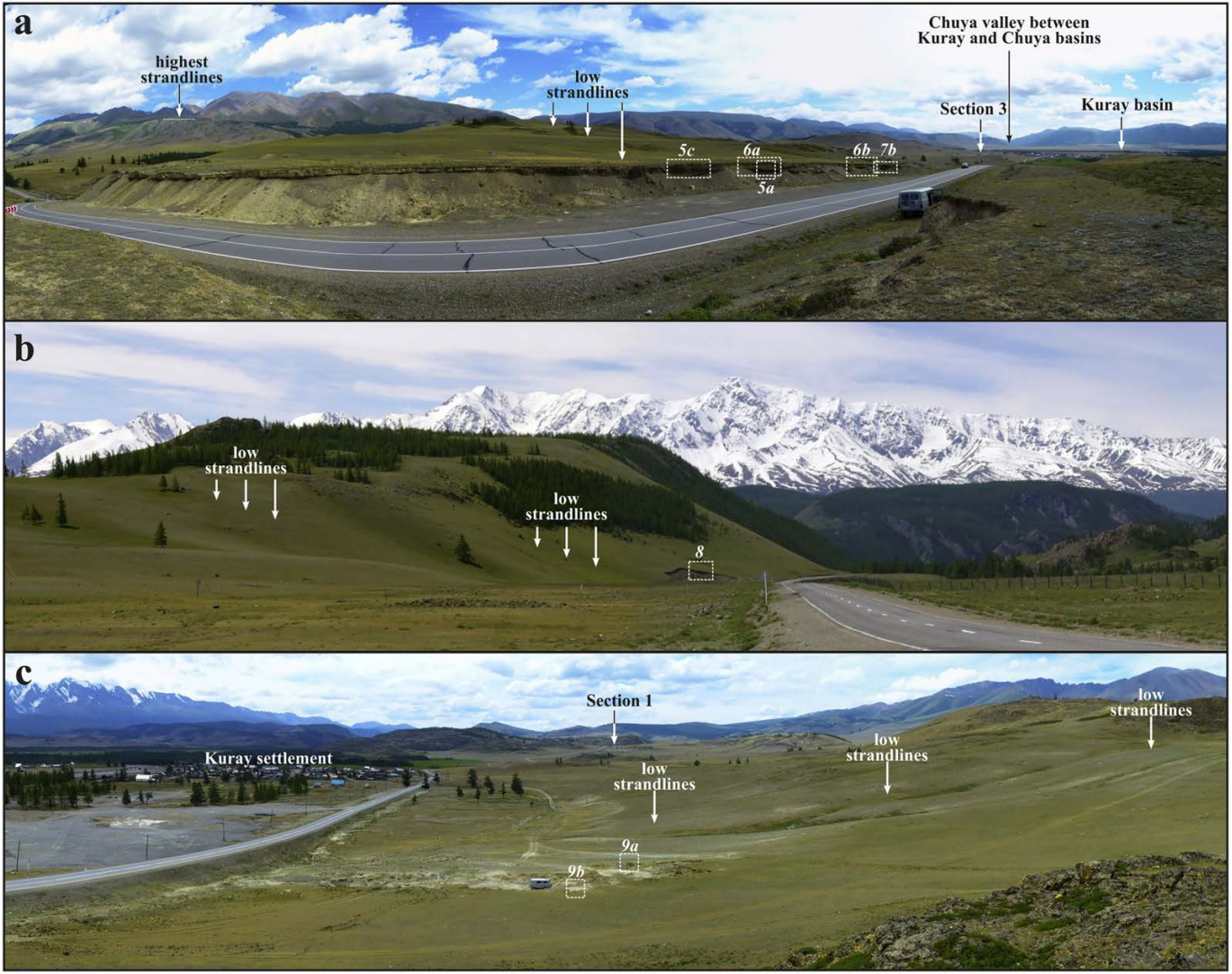
a
highest strandlines
low strandlines
Chuya valley between Kuray and Chuya basins
Section 3
Kuray basin
5c
6a
5a
6b
7b
b
low strandlines
low strandlines
8
c
Section 1
Kuray settlement
low strandlines
low strandlines
low strandlines
9a
9b

Figure 4

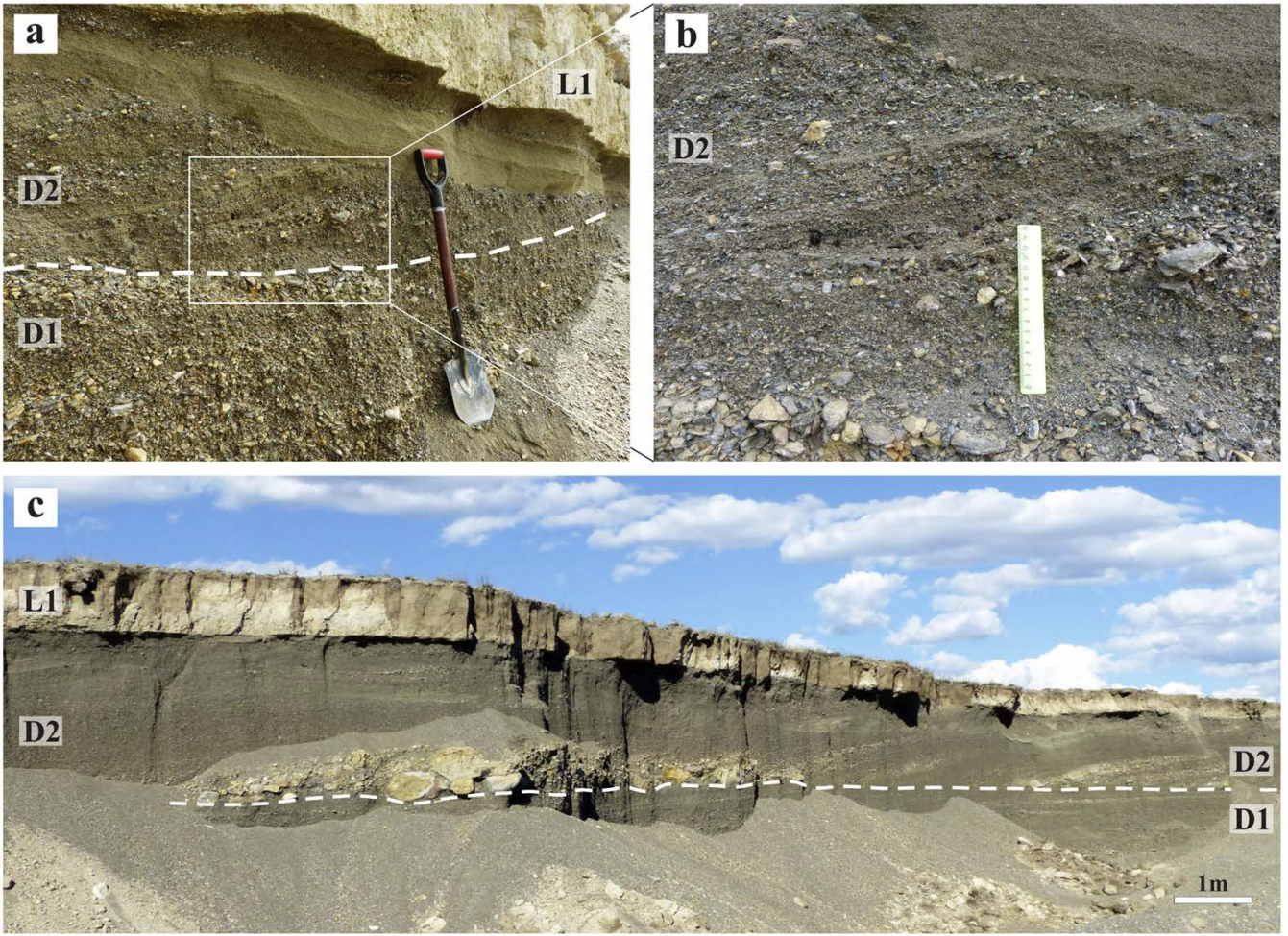

Figure 5

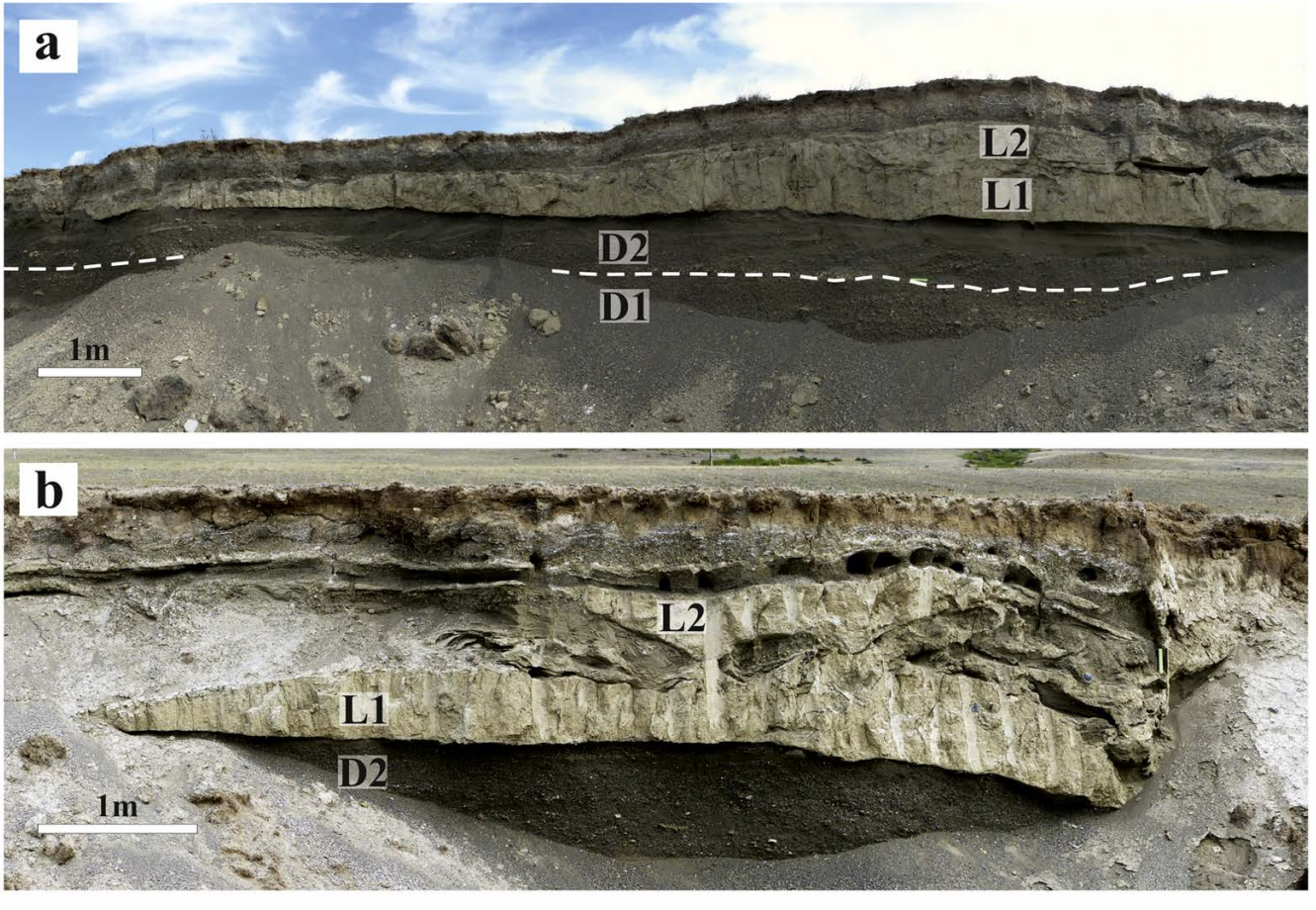

Figure 6

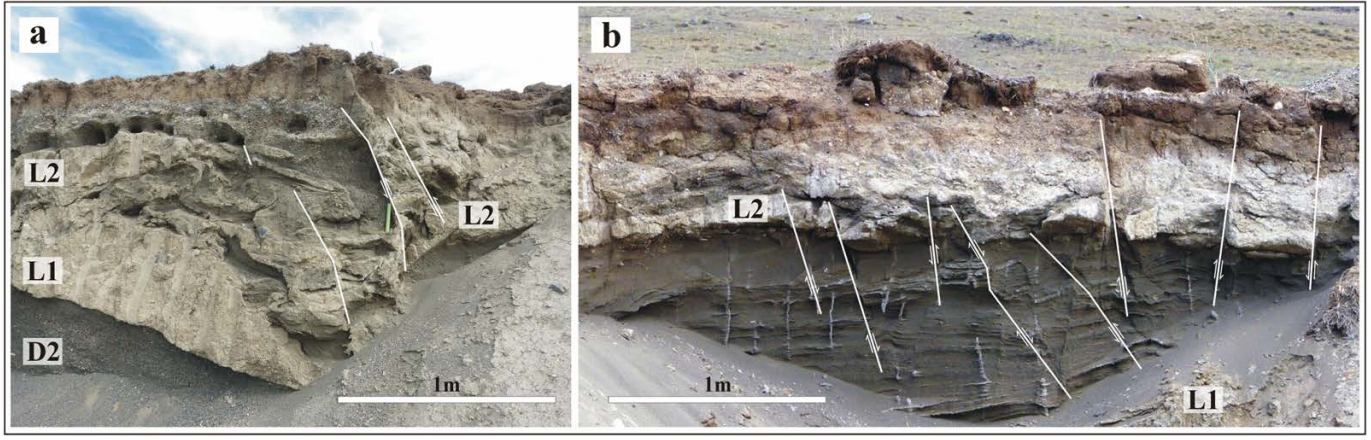

Figure 7

Figure 8

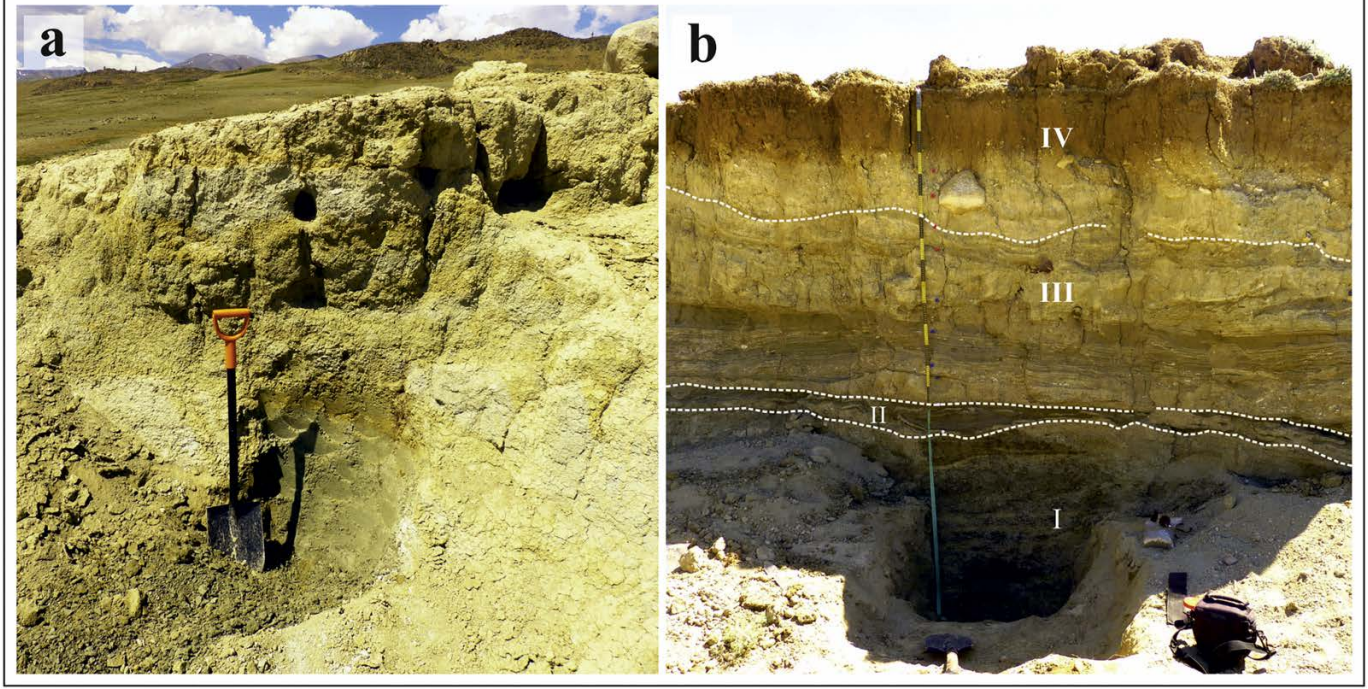

Figure 9

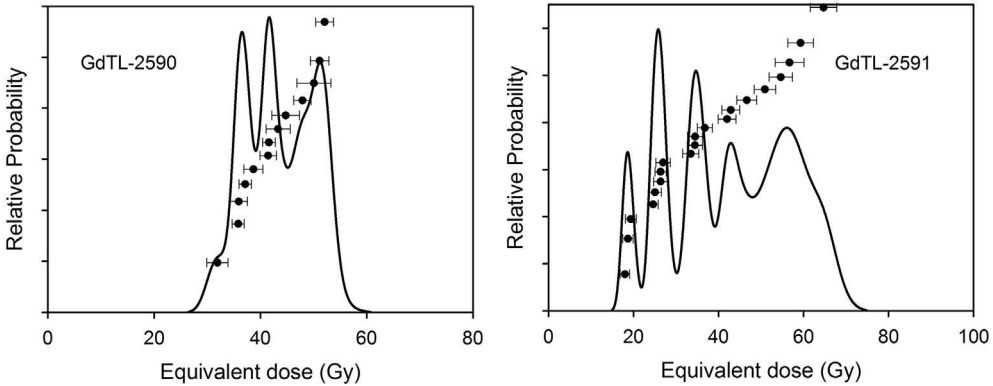
GdTL-2590
Relative Probability
0
20
40
60
80
Equivalent dose (Gy)
GdTL-2591
Relative Probability
0
20
40
60
80
100
Equivalent dose (Gy)

Figure 10

Figure 11

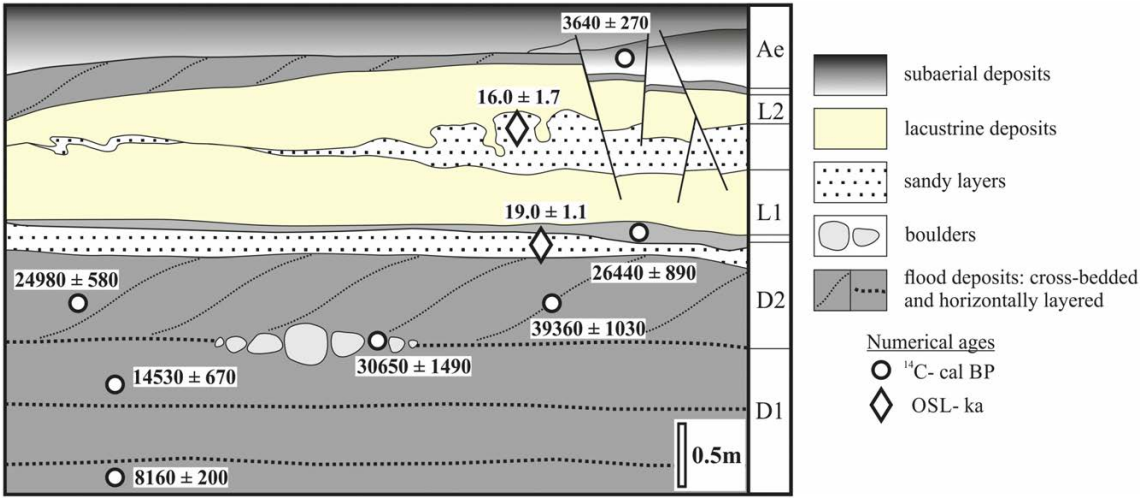
3640 ± 270
16.0 ± 1.7
19.0 ± 1.1
24980 ± 580
26440 ± 890
39360 ± 1030
30650 ± 1490
14530 ± 670
8160 ± 200
0.5m
Ae
L2
L1
D2
D1
subaerial deposits
lacustrine deposits
sandy layers
boulders
flood deposits: cross-bedded and horizontally layered
Numerical ages
14C- cal BP
OSL- ka

Figure 12

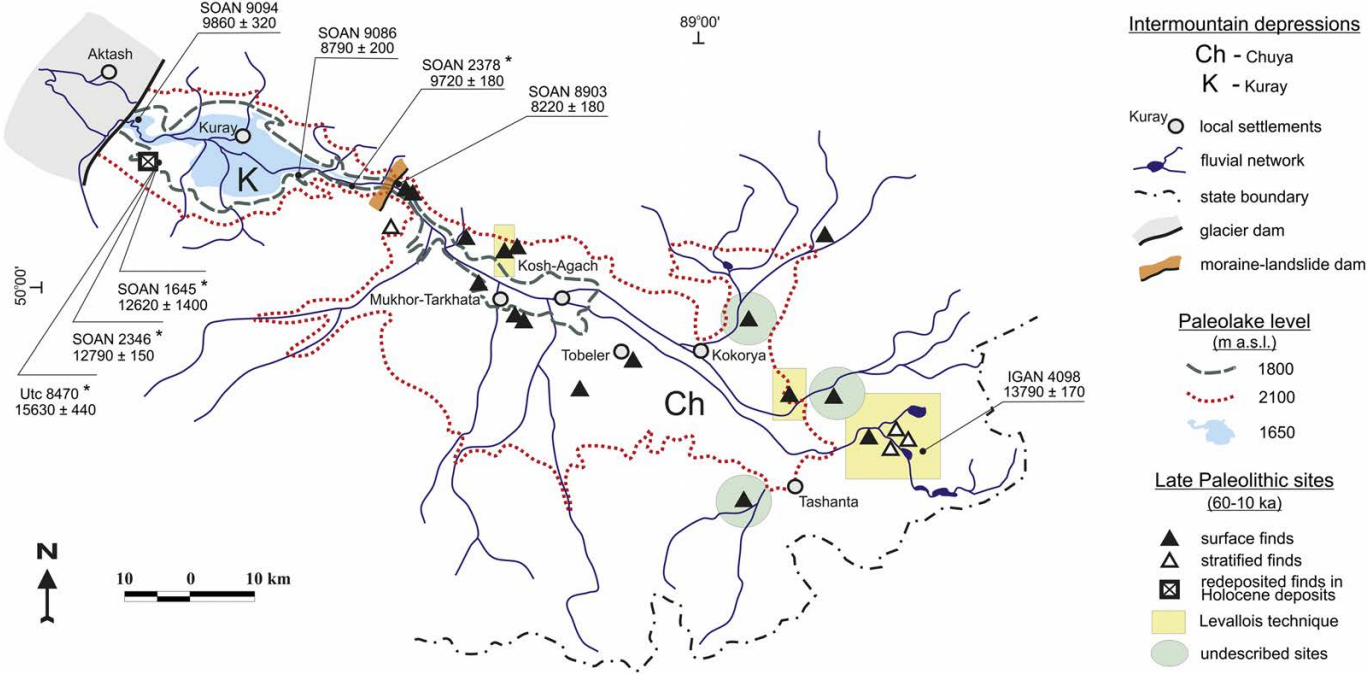
SOAN 9094
9860 ± 320
SOAN 9086
8790 ± 200
SOAN 2378 *
9720 ± 180
SOAN 8903
8220 ± 180
Aktash
Kuray
K
89°00'
50°00'
SOAN 1645 *
12620 ± 1400
SOAN 2346 *
12790 ± 150
Utc 8470 *
15630 ± 440
Kosh-Agach
Mukhor-Tarkhata
Tobeler
Kokorya
Ch
IGAN 4098
13790 ± 170
Tashanta
N
10 0 10 km
Intermountain depressions
Ch - Chuya
K - Kuray
Kuray local settlements
fluvial network
state boundary
glacier dam
moraine-landslide dam
Paleolake level
(m a.s.l.)
1800
2100
1650
Late Paleolithic sites
(60-10 ka)
surface finds
stratified finds
redeposited finds in Holocene deposits
Levallois technique
undescribed sites

Figure 13

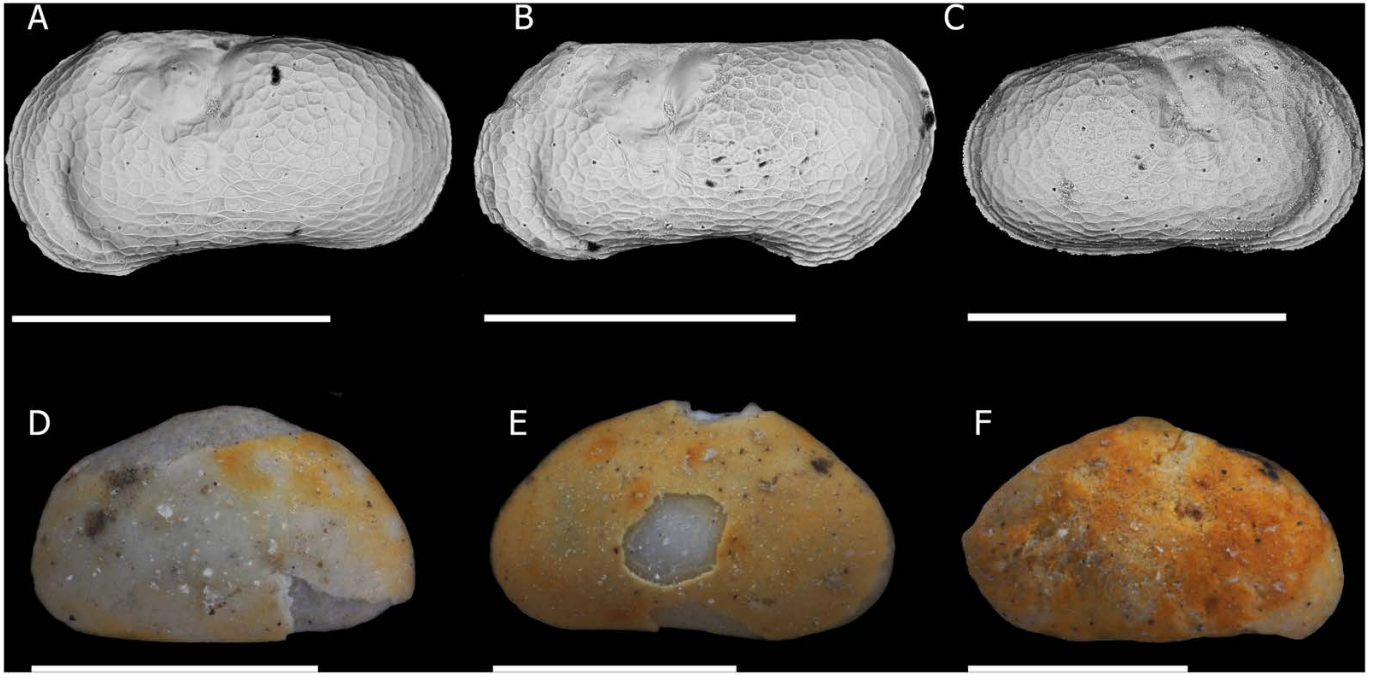

Figure 14

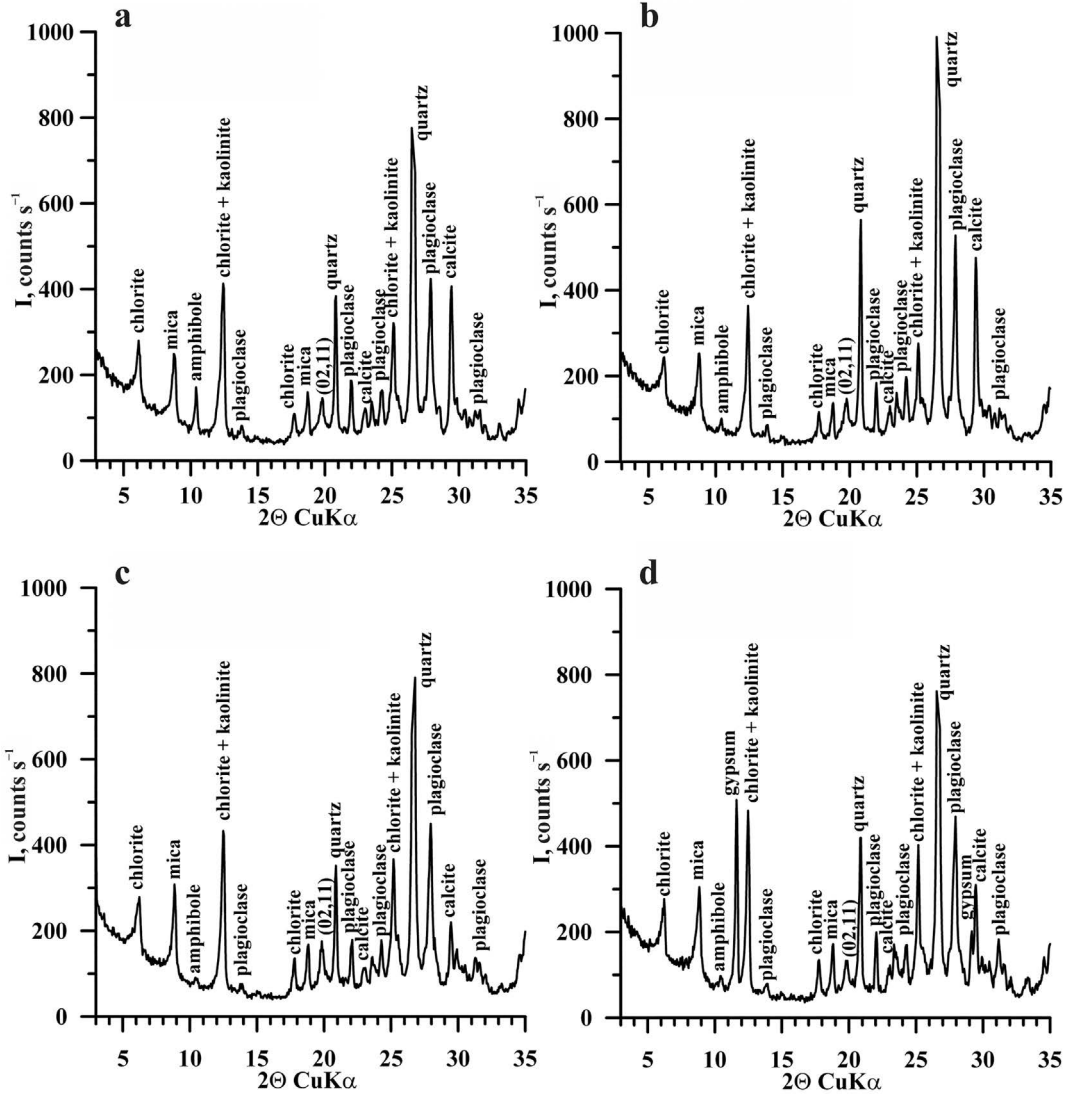
a
b
c
d
I, counts s⁻¹
2Θ CuKα
chlorite
mica
amphibole
chlorite + kaolinite
plagioclase
quartz
calcite
gypsum
(02,11)

Figure 15

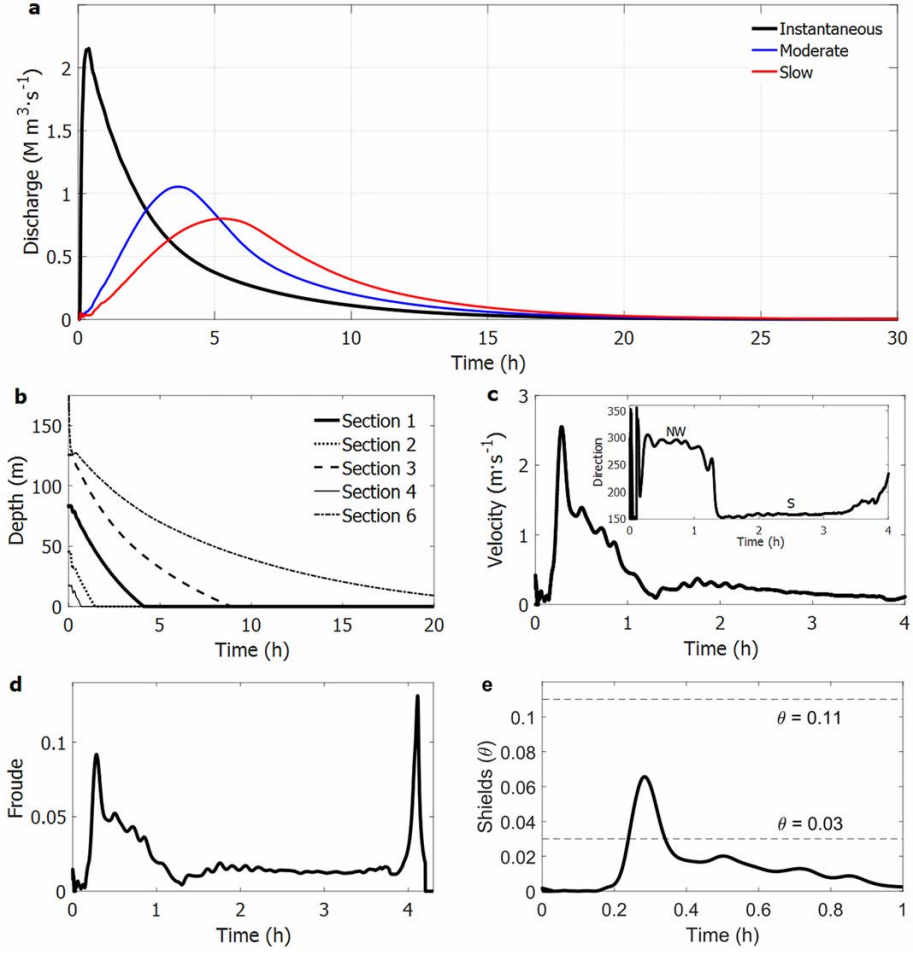
a
Instantaneous
Moderate
Slow
Discharge (M m3·s-1)
Time (h)
b
Section 1
Section 2
Section 3
Section 4
Section 6
Depth (m)
Time (h)
c
Velocity (m·s-1)
Direction
NW
S
Time (h)
Time (h)
d
Froude
Time (h)
e
θ = 0.11
θ = 0.03
Shields (θ)
Time (h)

Figure 16

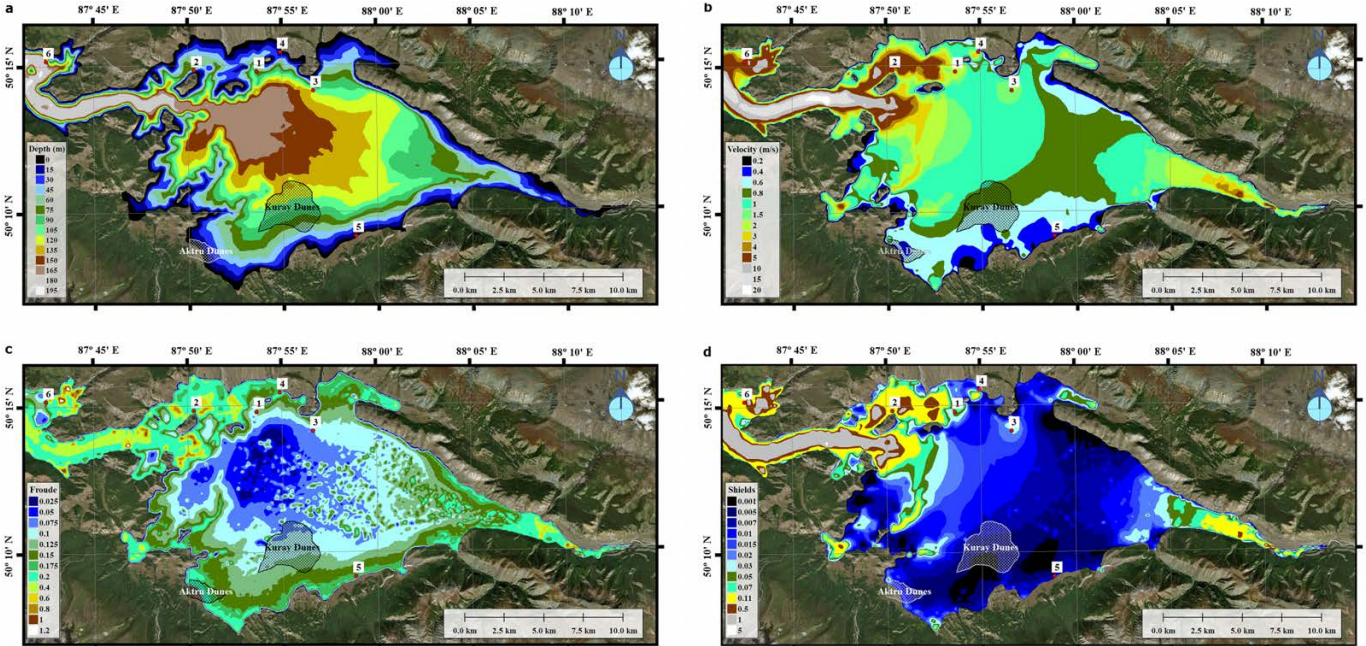
a
b
c
d
87° 45' E
87° 50' E
87° 55' E
88° 00' E
88° 05' E
88° 10' E
50° 15' N
50° 10' N
Depth (m)
0
15
30
45
60
75
90
105
120
135
150
165
180
195
Velocity (m/s)
0.2
0.4
0.6
0.8
1
1.5
2
3
4
5
10
15
20
Froude
0.025
0.05
0.075
0.1
0.125
0.15
0.175
0.2
0.4
0.6
0.8
1
1.2
Shields
0.001
0.005
0.007
0.01
0.015
0.02
0.03
0.05
0.07
0.11
0.5
1
5
Kuray Dunes
Aktru Dunes
1
2
3
4
5
6
0.0 km
2.5 km
5.0 km
7.5 km
10.0 km
N

Figure 17

Table 1. *Radiocarbon ages for organic material collected in sections 1, 4, 6, and previously published dates specifying the chronology of the last ice-dammed lakes in Chuya-Kuray system of intermountain depressions. All ^{14}C ages are obtained by LSC techniques. The samples marked with □ indicate apparent ^{14}C ages, and with * indicate ^{14}C ages were calibrated (2σ) in this paper.*

Lab code	Sample location	Altitude, m a.s.l.	^{14}C age, years BP	Calibrated (2σ) age, cal BP	Sample description
SOAN 9496	Section 1 (outcrop 6b, Fig. 4a)	1570	3380 ± 115	3640 ± 270	Fossil soil in subaerial pack above lacustrine deposits (Fig. 10)
SOAN 9502 □	Section 1 (outcrop 6a, Fig. 4a)	1570	22070 ± 450	26440 ± 890 □	Inclusions of peat in the upper part of upper diluvial pack (D2 in Fig.5a, Fig. 10)
SOAN 7802 □	Section 1 (outcrop 5a, Fig. 4a)	1570	34750 ± 480	39360 ± 1030 □	Inclusions of organic matter in the middle part of upper diluvial pack (D2 in Fig.5b, Fig. 10) (after Nazarov in Agatova et al., 2017b)
SOAN 4971 □	Section 1 (outcrop 6a, Fig. 4a)	1570	20750 ± 220	24980 ± 580 □	Fragment of charcoal in the middle part of upper diluvial pack (D2, Fig. 10) after (Vysotsky, 2009)
SOAN 9503 □	Section 1 (outcrop 5c, Fig. 4a)	1570	26715 ± 700	30650 ± 1490 □	Inclusions of peats at the bottom of the upper diluvial pack (D2 in Fig.6c, Fig. 10)
SOAN 9306 □	Section 1 (outcrop 6a, Fig. 4a)	1570	12400 ± 195	14530 ± 670 □	Organic fragments in the lower diluvial pack (D1, Fig. 10) (after Vysotsky in Agatova et al., 2019b)
SOAN 9305 □	Section 1 (outcrop 6a, Fig. 4a)	1570	7320 ± 110	8160 ± 200 □	Organic fragments in the lower diluvial pack (D1, Fig. 10) (after Vysotsky in Agatova et al., 2019b)
IGAN 4811 □	Section 4 (Fig. 3)	1646	35090 ± 950	39460 ± 2140 □	Peat layer in the Oligocene-Miocene deposits
SOAN 8681	Section 6 (Fig. 3)	1475	5650 ± 90	6470 ± 180	Upper horizon of fossil soil within colluvial deposits (Agatova et al., 2016)
SOAN 9094	Section 6 (Fig. 3)	1475	8770 ± 140	9860 ± 320	Lower horizon of fossil soil within colluvial deposits (Agatova et al., 2016)
SOAN 9086	Fig. 13	1720	7910 ± 70	8790 ± 200	Lower horizon of fossil soil above alluvial deposits (Agatova et al., 2017b)
SOAN 8903	Fig. 13	1730	7440 ± 95	8220 ± 180	Fossil soil above lacustrine deposits covered moraines (Agatova et al., 2016)
IGAN 4098	Fig. 13	2500	11910 ± 70	13790 ± 170	Paleopeat above moraines indicate deglaciation (Agatova et al., 2016)
SOAN 2378*	Fig. 13	1650	8700 ± 65	9720 ± 180*	Sediments of local landslide-dammed lake above diluvial deposits (Butvilovsky, 1993)
SOAN 1645*	Fig. 13	1754	10960 ± 550	12620 ± 1400*	Tree fragment in lacustrine deposits (Rusanov and Orlova, 2013)
SOAN 2346*	Fig. 13	1754	10845 ± 80	12790 ± 150*	Detritus in lacustrine deposits (Butvilovsky, 1993)
Utc 8470*	Fig. 13	1754	13050 ± 150	15630 ± 440*	Charcoal in lacustrine deposits indicate deglaciation (Blyakharchuk et al., 2008)
SOAN 3139*	Fig. 2	1600	17370 ± 550	21010 ± 1320*	Large fragment of travertine in diluvial deposits (after Butvilovsky in Rusanov and

					Orlova, 2013)

Table 2. *OSL ages for samples collected from Section 1, and previously published OSL age of lacustrine loams from Section 5 (Fig. 4). The dose rate was determined based on radioisotope content measurements. Final values of the dose rate were obtained for water content 18 ± 5%. The equivalent doses were calculated using central age model (CAM) of Galbraith et al. (1999).*

Sample ID	**Sample location**	**Depth (m)**	**U (Bq/kg)**	**Th (Bq/kg)**	**K (Bq/kg)**	**Dose rate (Gy/ka)**	**Equivalent dose (Gy)**	**OSL Age (ka)**	**Number of measured aliquots**	**Sample description**
GdTL-2590	Section 1	1.1	29.1±0.8	22.4±0.5	434±14	2.21±0.08	42.0±1.8	19.0±1.1	13	Sandy layer at the top of the D2 pack (Fig. 10)
GdTL-2591	Section 1	0.9	25.3±0.6	20.0±0.4	485± 15	2.23±0.08	35.9±3.5	16.0±1.7	20	Sandy layer between L2 and L1 packs (Fig. 10)
GdTL-2014	Section 5	1.2	N/A	N/A	N/A	N/A	N/A	18.2±1.1	N/A	Sands within strandline deposits (Panin et al., 2015b)